

Gö-VIP-27: Francesca Odoardi & Alexander Flügel

Name der Einrichtung: Institut für Neuroimmunologie und Multiple-Sklerose-Forschung, Universitätsmedizin Göttingen

Titel der Publikation: The lung microbiome regulates brain autoimmunity.

In: *Nature* **603**, 138–144 (2022)

Autoren: Leon Hosang¹, Roger Cugota Canals¹, Felicia Joy van der Flier¹, Jacqueline Hollensteiner², Rolf Daniel², Alexander Flügel^{1*#} & Francesca Odoardi^{1,3*#}

- (1) Institut für Neuroimmunologie und Multiple-Sklerose-Forschung (IMSF)
Universitätsmedizin Göttingen
Von-Siebold-Str. 3a
37075 Göttingen
 - (2) Abteilung für Genomische und Angewandte Mikrobiologie
Institut für Mikrobiologie und Genetik
Universität Göttingen
Grisebachstr. 8
37077 Göttingen
 - (3) Center for Biostructural Imaging of Neurodegeneration (BIN)
Universitätsmedizin Göttingen
Von-Siebold-Str. 3a
37075 Göttingen
- * contributed equally
corresponding authors

Zusammenfassung des wissenschaftlichen Inhalts

(Francesca Odoardi & Alexander Flügel)

Um uns mit Sauerstoff zu versorgen, ist die Lunge über eine große Austauschfläche mit der Umgebung verbunden, welche eine spezielle mikrobielle Flora beherbergt. In dieser Studie konnte eine enge Beziehung zwischen dem Lungenmikrobiom und der Immunreaktivität des Gehirns identifiziert werden. So scheint das Lungenmikrobiom die Aktivität der Mikroglia, der „Immunzellen des Gehirns“ zu regulieren, indem es als eine Art Frühwarnsystem wirkt. Die Relevanz dieser „Lunge-Hirn-Achse“ konnte in einem Tiermodell der multiplen Sklerose, einer Autoimmunerkrankung des Gehirns, demonstriert werden:

Eine leichte Manipulation der mikrobiellen Flora durch lokale Gabe eines niedrigdosierten Antibiotikums reichte aus, um die Anfälligkeit des Gehirns für diese Autoimmunerkrankung zu verändern. Nach der Antibiotikagabe waren die Verästelungen der Mikroglia verkürzt und sie reagierten weniger auf Entzündungsreize. Eine Analyse des behandelten Lungenmikrobioms ergab, dass sich bestimmte Bakterien verstärkt im Lungengewebe ansammeln, die einen besonderen Zellwandbestandteil, nämlich Lipopolysaccharid (LPS), produzieren. Tatsächlich

konnte die Behandlung der Tiere mit den inaktivierten Bakterien oder ihrem LPS den bei der Antibiotikabehandlung beobachteten Phänotyp rekapitulieren.

Diese neuentdeckte Lunge-Hirn-Achse könnte auch aus klinischer Sicht relevant sein: Infektionen der Lunge, Rauchen, und Umweltfaktoren können sich auf das Lungenmikrobiom auswirken und somit die Immunreaktion des Gehirns beeinflussen. Diese enge Verbindung von Lunge und Gehirn könnte möglicherweise therapeutisch genutzt werden, z. B. durch lokale Gabe bestimmter Probiotika oder Antibiotika. Eine gezielte Beeinflussung der Immunreaktivität des Gehirns ist darüber hinaus bei der Behandlung einer Vielzahl von infektiösen oder degenerativen Erkrankungen des zentralen Nervensystems denkbar.

Weitere Informationen:

Prof. Dr. Francesca Odoardi & Prof. Dr. Alexander Flügel

Universitätsmedizin Göttingen

Institut für Neuroimmunologie und Multiple Sklerose Forschung

Anschrift: Von-Siebold-Str. 3a, 37075 Göttingen

Telefon: 0551/61158

Email: IMSF@med.uni-goettingen.de

The lung microbiome regulates brain autoimmunity

<https://doi.org/10.1038/s41586-022-04427-4>

Received: 15 September 2020

Accepted: 17 January 2022

Published online: 23 February 2022

 Check for updates

Leon Hosang¹, Roger Cugota Canals¹, Felicia Joy van der Flier¹, Jacqueline Hollensteiner², Rolf Daniel², Alexander Flügel^{1,4}✉ & Francesca Odoardi^{1,3,4}✉

Lung infections and smoking are risk factors for multiple sclerosis, a T-cell-mediated autoimmune disease of the central nervous system¹. In addition, the lung serves as a niche for the disease-inducing T cells for long-term survival and for maturation into migration-competent effector T cells². Why the lung tissue in particular has such an important role in an autoimmune disease of the brain is not yet known. Here we detected a tight interconnection between the lung microbiota and the immune reactivity of the brain. A dysregulation in the lung microbiome significantly influenced the susceptibility of rats to developing autoimmune disease of the central nervous system. Shifting the microbiota towards lipopolysaccharide-enriched phyla by local treatment with neomycin induced a type-I-interferon-primed state in brain-resident microglial cells. Their responsiveness towards autoimmune-dominated stimulation by type II interferons was impaired, which led to decreased proinflammatory response, immune cell recruitment and clinical signs. Suppressing lipopolysaccharide-producing lung phyla with polymyxin B led to disease aggravation, whereas addition of lipopolysaccharide-enriched phyla or lipopolysaccharide recapitulated the neomycin effect. Our data demonstrate the existence of a lung–brain axis in which the pulmonary microbiome regulates the immune reactivity of the central nervous tissue and thereby influences its susceptibility to autoimmune disease development.

Autoimmune processes of the central nervous system (CNS) not only depend on local conditions in the nervous tissue itself, but are also controlled by peripheral organ systems. Of the latter, the lung seems to have an important role. Smoking and lung infections substantially increase the likelihood of multiple sclerosis¹. In addition, activated T cells—which can trigger an autoimmune reaction within the CNS—migrate into the lung tissue, where they develop into migration-competent pathogenic effector cells and survive as long-term memory cells². The lung is characterized by a specialized milieu with an individual microbial flora. This pulmonary microbiota contributes to the regulation of local immune responses in pathological processes such as asthma, idiopathic pulmonary fibrosis or tumour^{3,4}. We here wanted to find out if autoimmune processes of the brain can also be influenced by the lung microbial communities.

We began by investigating whether the lung microbiota affects the initiation of an autoimmune process inside the lung. For this purpose, we specifically manipulated the microbiota in the lung and established a rat model of lung experimental autoimmune encephalomyelitis (lung EAE) (Extended Data Fig. 1a). Daily intratracheal infusion of 1 mg neomycin induced significant changes in lung microbiome diversity and abundance (Fig. 1a) without measurable alterations to the lung-intrinsic cellular immune milieu (Extended Data Fig. 1b–f). Into these pre-treated rats we intravenously transferred myelin basic

protein (MBP)-specific T cells (T_{MBP} cells) and then, 6 h later, immunized the rats intratracheally with MBP. Of note, after the neomycin treatment, the lung EAE was almost completely blocked. By contrast, rats that did not receive neomycin developed ‘classical’ EAE (Fig. 1b).

Neomycin applied this way should only act locally in the lung tissue. We wanted to exclude, though, that our observed clinical effects could have been caused by some of the antibiotic drug spilling over from the airways to the gastrointestinal tract and changing the intestinal microbiota, as the intestinal microbiome can substantially influence immune responses, including autoimmune processes of the CNS^{5–9}. However, analyses of the gut microbiota after intratracheal treatment with neomycin did not show any significant changes in diversity or abundance of the commensal gut bacterial strains (Fig. 1c). Moreover, a direct application of neomycin into the gastrointestinal tract at the dose used for the intratracheal applications induced only minimal changes in the gut microbiome and, importantly, was not sufficient to ameliorate clinical EAE (Extended Data Fig. 2a, b). At 10-fold-higher doses of neomycin, changes in the microbiome diversity of the gut emerged, but no effects on EAE were observed in this set-up either (Extended Data Fig. 2a, b).

The disease-ameliorating effects of neomycin might theoretically be explained by a direct suppressive effect on the effector T cells rather than by its antibiotic potential. However, even exposing T cells to 10-fold-higher concentrations of neomycin than those used in our *in vivo* applications

¹Institute for Neuroimmunology and Multiple Sclerosis Research, University Medical Center Göttingen, Göttingen, Germany. ²Department of Genomic and Applied Microbiology, University of Göttingen, Göttingen, Germany. ³Center for Biostructural Imaging of Neurodegeneration, University Medical Center Göttingen, Göttingen, Germany. ⁴These authors contributed equally: Alexander Flügel, Francesca Odoardi. ✉e-mail: fluegel@med.uni-goettingen.de; odoardi@med.uni-goettingen.de

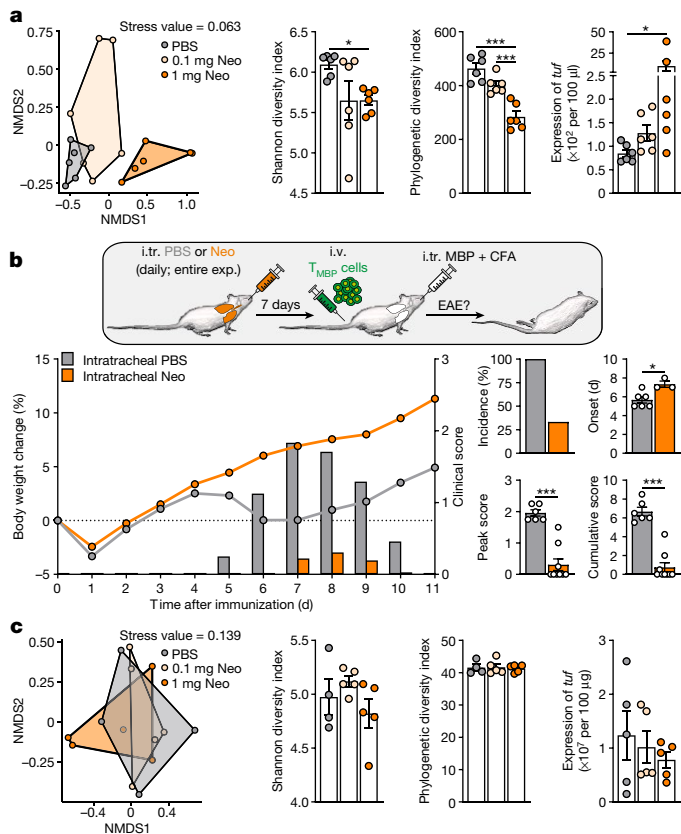


Fig. 1 | Manipulations of the lung microbiota affect CNS autoimmunity. **a**, Intratracheal treatment with neomycin (Neo) induces lung microbiota dysbiosis. Left, principal component analysis (PCA) of the microbiota composition of BALF from rats that were intratracheally treated with PBS or neomycin at the indicated concentration for 7 days. 16S rRNA sequencing (NMDS, non-metric multidimensional scaling). Middle, corresponding Shannon and phylogenetic diversity indices. Right, quantification of bacterial abundance based on *tuf* gene expression via 16S rRNA-based quantitative PCR. Mean \pm s.e.m. Cumulative data from two independent experiments. $n = 6$ (all groups). **b**, Intratracheal (i.t.) treatment with neomycin ameliorates active EAE. Lung EAE was induced in rats that were pre-treated intratracheally with neomycin or PBS for 7 days. Clinical parameters: Body weight change (lines) and clinical scores (bars) over the EAE course, incidence (%), average onset (days after immunization), average peak score, average cumulative score. Mean \pm s.e.m. Representative data from four independent experiments. $n = 6$ (PBS); $n = 9$ (Neo). CFA, complete Freund's adjuvant; i.v., intravenous. **c**, Intratracheal treatment with neomycin does not induce gut microbiota dysbiosis. PCA, Shannon and phylogenetic diversity indices and quantification of bacterial abundance in faecal samples from the same rats as in **a**. Mean \pm s.e.m. $n = 4$ (PBS); $n = 5$ (0.1 and 1 mg Neo). **a, c**, Statistical significance by one-way ANOVA with Tukey's multiple comparisons test (Gaussian distribution) and Kruskal–Wallis test with Dunn's multiple comparisons test (non-Gaussian distribution). **b**, Statistical significance by unpaired two-tailed *t*-test (Gaussian distribution) and Mann–Whitney test (non-Gaussian distribution). * $P < 0.05$, *** $P < 0.001$.

did not influence their proliferation or their encephalitogenic potential (Extended Data Fig. 2c, d). Furthermore, the presence of the lung microbiota was essential for the neomycin effect; application of neomycin in a location that lacks a microbial environment—that is, subcutaneous injection—did not influence EAE, regardless of whether the disease was induced by intratracheal or subcutaneous immunization (Extended Data Fig. 2e, f).

T cell function with microbiome dysbiosis

The data up to this point suggested that dysregulation of the local microbiota can have a considerable effect on the generation of autoimmune

processes in the lung. To confirm this, we tracked fluorescently labelled effector T cells (T_{MBP} cells)¹⁰ in the course of the lung EAE model. We did not see any effects of local neomycin treatment on the amplification of the T cells within the lung after the intratracheal immunization, nor was there any change in their consequent entry into the blood. However, there was a significant reduction of T_{MBP} cells within the CNS tissue (Fig. 2a). This reduced accumulation of effector T cells within the CNS tissue could not be explained by intrinsic changes in their differentiation or activation state within the lung. Global expression profiles of T_{MBP} cells retrieved from neomycin-treated and control rats revealed that the profound transcriptional changes of T_{MBP} cells after immunization in both treated and control rats were virtually identical (Fig. 2b, Extended Data Fig. 3a–d). Quantitative PCR for genes that encode relevant cytokines, chemokine receptors and factors controlling T cell division and egression confirmed these data (Fig. 2c, Extended Data Fig. 3e). We also did not detect any significant changes in numbers or differentiation of the other immune cell populations in the lung (Extended Data Fig. 4a–f).

These data indicated that the disease-suppressing effects of the neomycin-manipulated lung microbiota could not be explained by an influence on the activation process of the T_{MBP} cells within the lung tissue. We therefore tested whether EAE induced outside of the lung—that is, by subcutaneous immunization—could also be influenced by manipulating the lung microbiome. Indeed, this 'peripheral EAE' was significantly ameliorated after intratracheal treatment with neomycin (Extended Data Fig. 4g). Furthermore, we observed a significant disease-dampening effect when EAE was induced by the transfer of effector T cells (transfer EAE); that is, in a situation in which immunization and a consecutive activation of the T cells in situ are not required (Fig. 2d). To confirm the role of the lung microbiota in this EAE model, we performed a bacterial transfer experiment. We discontinued the intratracheal neomycin treatments of rats and 'substituted' the neomycin with daily intratracheal transfers of microbiota isolated from the bronchoalveolar lavage fluid (BALF). Notably, we observed a significant reduction of the clinical symptoms of transfer EAE in the rats that had received BALF-microbiota from neomycin-treated rats but not in those that had received BALF-microbiota from control rats (Fig. 2e).

To determine by which mechanisms the modified lung microbiome interferes with the autoimmune processes we tracked the pathogenic T_{MBP} cells in the course of both peripheral and transfer EAE. The T cell numbers and their preclinical migration patterns in the periphery were not affected by the antibiotic treatment. Instead, similarly to neomycin treatment in lung EAE, we found that the numbers of the T_{MBP} cells within the CNS tissue were significantly reduced (Fig. 2f–h, Extended Data Fig. 4h).

The neomycin-induced changes of the lung microbiome did not only influence classical T_{MBP} -cell-induced EAE, which preferentially affects the spinal cord white matter. An autoimmune disease of the grey matter of the brain evoked by the transfer of β -synuclein-reactive T cells (T_{bSYN} cells)¹¹ was likewise ameliorated. Also in this set-up, the accumulation of pathogenic T_{bSYN} cells in the cortical grey matter of the brain was reduced in neomycin-treated rats, indicating that changes in the microbiome affect autoimmune responses in the entirety of the CNS tissues (Extended Data Fig. 4i, j).

These data suggest that the manipulation of the lung microbiome does not affect the T-cell-triggered autoimmune process in the periphery, but rather that it has an effect at the border of or within the CNS. Next, therefore, we investigated the interaction of the effector T cells with the endothelium of the blood–brain barrier (BBB). T_{MBP} cells enter the CNS tissue from leptomeningeal vessels of the spinal cord, where they crawl on the endothelial surface using integrins and chemokines as adhesion factors^{12,13}. Treatment with neomycin did not change the expression of these relevant adhesion molecules in T_{MBP} cells, either in active or in transfer EAE (Extended Data Fig. 5a, b).

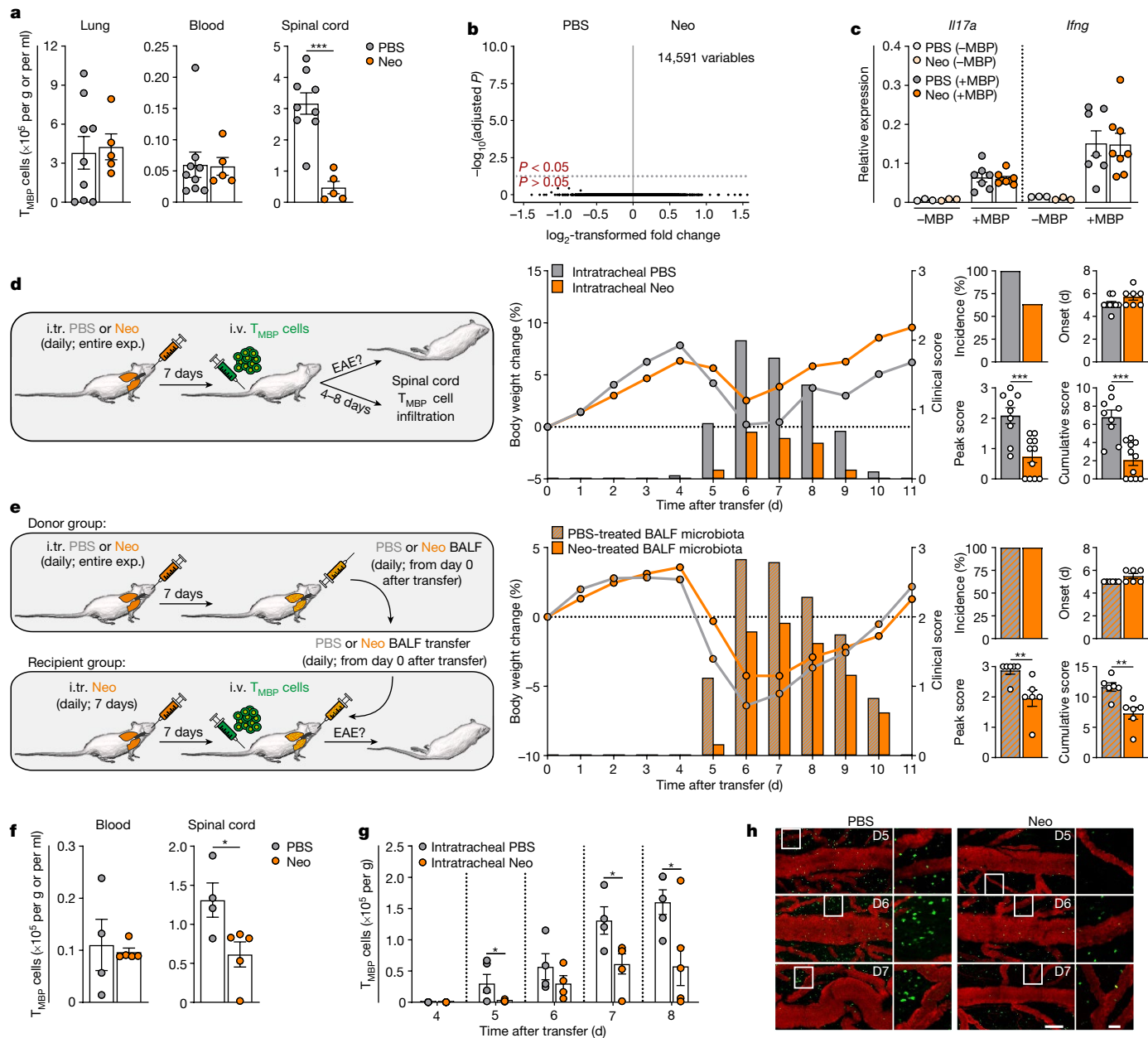


Fig. 2 | Lung dysbiosis does not influence T cell activation and migration. **a–c**, Lung EAE was induced in rats that were pre-treated intratracheally with neomycin or PBS for 7 days. **a**, Neomycin treatment reduces CNS invasion but not the peripheral T cell distribution. Number of T_{MBP} cells. Flow cytometry. Day 7 after immunization. Mean \pm s.e.m. Cumulative data from two independent experiments. $n = 9$ (PBS); $n = 5$ (Neo). **b**, **c**, Intratracheal treatment with neomycin does not change the T cellular transcriptome. **b**, Differential gene expression of T_{MBP} cells from lungs on day 1 after immunization in rats that were pre-treated with PBS versus neomycin. **c**, Cytokine expression of T_{MBP} cells in the lungs of rats that were immunized with MBP (+MBP; $n = 8$ per group) or without MBP (–MBP; $n = 3$ per group). Quantitative PCR. Day 1 after immunization. Mean \pm s.e.m. Cumulative data from two independent experiments. **d**, Intratracheal treatment with neomycin ameliorates transfer EAE. Clinical parameters. Mean \pm s.e.m. Cumulative data from three independent experiments. $n = 9$ (PBS); $n = 11$ (Neo). **e**, The lung microbiota of neomycin-treated rats ameliorates EAE. Rats were intratracheally pre-treated with

neomycin. The treatment was interrupted before T_{MBP} cell transfer and continued through intratracheal transfer of microbiota isolated from BALF of rats that were intratracheally pre-treated with neomycin or PBS. Clinical parameters. Mean \pm s.e.m. Cumulative data from two independent experiments. $n = 6$ (both groups). **f–h**, Pre-treatment with neomycin reduces T_{MBP} cell entry into the spinal cord. **f**, Experimental setup as in Fig. 2d. Number of T_{MBP} cells. Day 7 after transfer. Mean \pm s.e.m. Representative data from three independent experiments. $n = 4$ (PBS); $n = 5$ (Neo). **g**, Kinetics of T_{MBP} cell invasion in the spinal cord. Flow cytometry. Mean \pm s.e.m. Representative data from two independent experiments. $n = 4–6$ (PBS); $n = 4–7$ (Neo) per time point. **h**, CNS invasion of T_{MBP} cells (green). Intravital TPLSM. Representative images from two independent experiments. Red, vessels. Scale bars, 100 μ m (main images); 50 μ m (magnified images). **a**, **c–g**, Statistical significance by unpaired two-tailed t -test (Gaussian distribution) and Mann–Whitney test (non-Gaussian distribution). * $P < 0.05$, ** $P < 0.01$, *** $P < 0.001$.

Moreover, intravital two-photon laser scanning microscopy (TPLSM) revealed that T_{MBP} cells exhibited the typical migratory pattern within leptomeningeal vessels (Extended Data Fig. 5c, Supplementary Video 1). To exclude any effects on the endothelium as a result of the different

inflammatory conditions of the CNS in neomycin-treated versus control rats, we tracked brain-antigen-ignorant ovalbumin-specific T cells (T_{OVA} cells). These cells also crawl within leptomeningeal vessels and transgress into the leptomeningeal milieu—although to a lesser extent

than T_{MBP} cells^{12,14}. Of note, the intra- and extravascular locomotion behaviour and diapedesis of the T_{OVA} cells were virtually identical after neomycin treatment (Extended Data Fig. 5d, e, Supplementary Video 2). Furthermore, the expression profiles from endothelial cells of neomycin-treated and control rats did not show significant regulation of genes that determine the barrier function or the adhesiveness of the vasculature (Extended Data Fig. 5f), and TPLSM did not provide any evidence for a leaky BBB (Extended Data Fig. 5g), indicating that the changes to the lung microbiome by neomycin did not influence the properties of the CNS endothelium.

The lung microbiota influences microglia

We next examined whether the initiation of the autoimmune process within the CNS tissue was changed after the neomycin treatment. After endothelial transmigration, T_{MBP} cells become reactivated within the CNS when they re-encounter their cognate antigen presented by local antigen-presenting cells (APCs)¹⁴. The consecutive T cellular release of cytokines—a classical type II interferon (IFN)-dominated profile—stimulates resident immune-competent cells and thereby triggers the recruitment of peripheral immune cells that induce structural damage and clinical signs^{11,15–18}. Longitudinal analyses in the course of EAE indeed revealed a significantly decreased inflammatory milieu in the CNS tissue of neomycin-treated rats (Fig. 3a, Extended Data Fig. 6a). This dampened autoimmune inflammation could not be explained by a failure of the T_{MBP} cells to become reactivated within the CNS tissue (Extended Data Fig. 6b, c). Neither could we find significant differences in the differentiation, relative numbers or cytokine expression of recruited immune cells (Extended Data Fig. 6). As the full manifestation of clinical signs occurs only after a secondary glial inflammatory response, we speculated that the transmission of the T cellular immune trigger within the tissue might be disturbed. Therefore, we next tested the functionality of microglia, the primary CNS-resident population of immune cells, which can react very sensitively to T cell-derived stimuli¹⁹; for example, by producing proinflammatory factors and chemokines and upregulating the expression of MHC-II molecules²⁰. We found that microglia in acute autoimmune lesions did not assume their characteristic activatory morphological transformation (Extended Data Fig. 7a). Furthermore, in contrast to the recruited myeloid cells, microglia showed reduced expression levels of CXCL9, CXCL10, CXCL11, inducible nitric oxide synthase (iNOS) and MHC-II (Fig. 3b, Extended Data Fig. 6d). The relevance of microglia in EAE pathogenesis and lung microbiome regulation was further supported by treating the rats with minocycline, which interferes with the activation of microglia²¹. We in fact observed a significant suppression of transfer EAE after application of minocycline (Fig. 3c). Notably, pre-treating the rats with neomycin did not add to the disease-dampening effect of minocycline (Fig. 3c). Very similar results were obtained when we targeted the microglia with an ablation strategy using a selective colony stimulating factor 1 receptor (CSF1R) inhibitor²² (Extended Data Fig. 7b, c). Although we cannot rule out that changes in the peripheral or recruited immune cells could contribute to the clinical effects, our data indicate that it is mainly the microglia that are influenced after the neomycin-induced lung microbiome dysbiosis and that mediate the altered autoimmune response.

Even in the absence of autoimmune inflammation, we noted a marked change in the microglial morphology after intratracheal treatment with neomycin, both in the spinal cord and in the brain cortical grey matter tissue. The lengths and numbers of their branches were significantly reduced, whereas the numbers of microglia were unchanged (Fig. 4a, Extended Data Fig. 7d–f, Supplementary Video 3). Global transcriptome analyses of microglia revealed significant transcriptional changes in a restricted number of genes; genes such as *Mx1*, *Mx2*, *Rsad2*, *Oas1a* and *Irf7* were upregulated, whereas *Il6st* and *Irf8* were downregulated (Fig. 4b and Supplementary Table 1). Gene Ontology (GO)

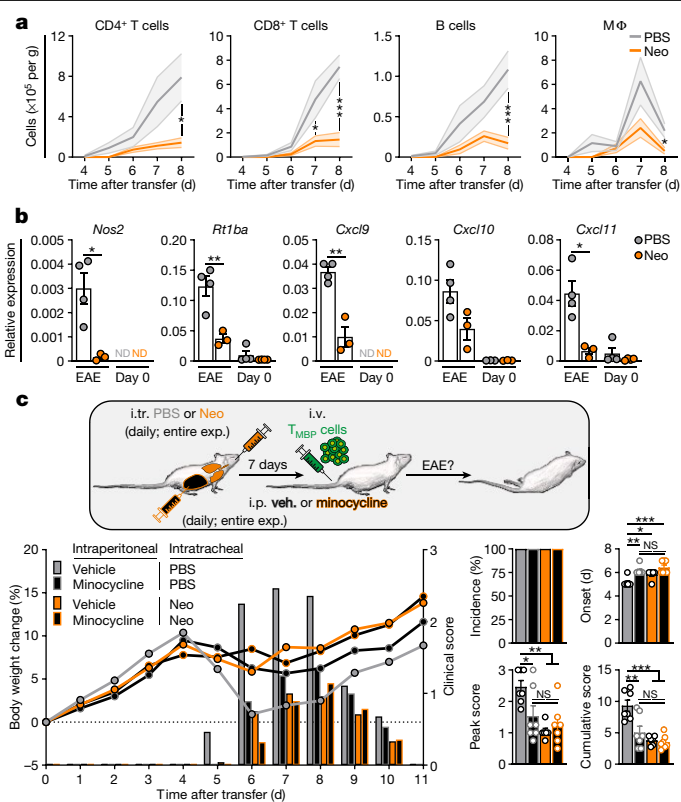


Fig. 3 | Lung dysbiosis affects microglia immune reactivity. a, b, EAE was induced in rats that were pre-treated intratracheally with neomycin or PBS by transfer of T_{MBP} cells. **a**, Intratracheal treatment with neomycin reduces T_{MBP} -cell-mediated CNS inflammation. Number of endogenous $\alpha\beta TCR^+$ $CD4^+$ and $CD8^+$ T cells, $CD45^{RA}$ B cells and $CD45^{high} CD11b^+$ MΦ (recruited monocytes and resident macrophages) isolated from the spinal cord at the indicated time points after transfer. Flow cytometry. Mean \pm s.e.m. Representative data from three independent experiments. $n = 4$ (PBS); $n = 4–6$ (Neo) per time point. **b**, Intratracheal treatment with neomycin dampens the microglial response to a T-cell-mediated attack. Differential expression of iNOS (*Nos2*), MHC-II (*Rtlba*) and chemokines in microglia sorted at the initiation stage of the EAE from PBS- or neomycin-treated rats. Quantitative PCR. Mean \pm s.e.m. Representative data from two independent experiments. $n = 4$ (PBS); $n = 3$ (Neo) per condition. ND, not detected. **c**, Minocycline ameliorates EAE but does not add to the disease-ameliorating effects of intratracheal neomycin treatment. Rats were treated intraperitoneally with minocycline or vehicle and intratracheally with neomycin or PBS. After 7 days, EAE was induced by T_{MBP} cell transfer. The treatments were continued throughout the entire disease course. Clinical parameters. Mean \pm s.e.m. Cumulative data from two independent experiments. $n = 7$ (vehicle + PBS, minocycline + PBS, minocycline + Neo); $n = 6$ (vehicle + Neo). i.p., intraperitoneal. **a, b**, Statistical significance by unpaired two-tailed *t*-test (Gaussian distribution) and Mann–Whitney test (non-Gaussian distribution). **c**, Statistical significance by one-way ANOVA with Tukey’s multiple comparisons test. * $P < 0.05$, ** $P < 0.01$, *** $P < 0.001$; NS, not-significant.

term analysis revealed that most of the upregulated genes could be attributed to the type I IFN signalling pathway (Extended Data Fig. 7g). The regulation of several of these genes was confirmed with quantitative PCR (Fig. 4c, Extended Data Fig. 7h). The genes that were changed in total tissue and microglia overlapped to a large extent, indicating that lung-microbiota-induced changes of the CNS tissue primarily affect the microglia (Fig. 4b, Extended Data Fig. 7i). Indeed, astrocytes—the other major immune-competent glial cell population of the CNS—did not show this shift towards a type I IFN signalling pathway (Extended Data Fig. 7j).

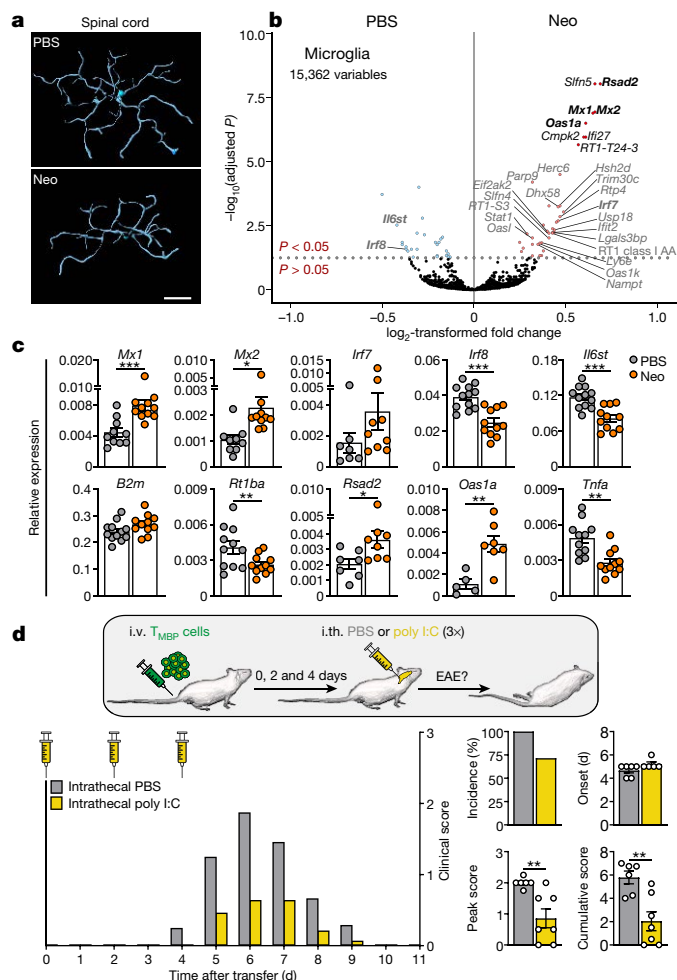


Fig. 4 | Lung dysbiosis shifts microglia to a type I IFN signature.

a, Intratracheal treatment with neomycin induces an altered microglia morphology. Confocal three-dimensional (3D) reconstructions of IBA1⁺ microglia in the grey matter of the spinal cord 7 days after intratracheal treatment with PBS or neomycin. Representative images of 16 different cells from 3 rats per group. Scale bar, 10 μ m. **b, c**, Intratracheal treatment with neomycin induces a type I IFN signature in spinal cord microglia. **b**, Comparison of global gene expression profile in CD45^{low}CD11b⁺ microglia sorted from the spinal cord of rats treated with PBS or neomycin for 7 days. Candidate genes upregulated in neomycin- versus PBS-treated rats are indicated as red dots. Genes significantly up- or downregulated ($P < 0.05$) but below the 0.5 fold change cut-off are indicated as light red and light blue dots, respectively. Type I IFN-regulated genes are indicated. Bold, genes confirmed by quantitative PCR. **c**, Set-up as in **b**. Expression of type I IFN-regulated genes measured by quantitative PCR. Mean \pm s.e.m. Cumulative data from three independent experiments. $n = 5$ –12 per condition (both groups). **d**, Intratracheal (i.th.) treatment with poly I:C ameliorates EAE. EAE was induced by transfer of T_{MBP} cells. Poly I:C was administered intrathecally on days 0, 2 and 4 after T_{MBP} cell transfer. Clinical parameters. Mean \pm s.e.m. Cumulative data from two independent experiments. $n = 6$ (both groups). **c, d**, Statistical significance by unpaired two-tailed t -test (Gaussian distribution) and Mann-Whitney test (non-Gaussian distribution). * $P < 0.05$, ** $P < 0.01$, *** $P < 0.001$.

It should be noted that a shift of microglial reactivity to a type I IFN immune reactivity can modulate microglial responsiveness towards the type II IFN-dominated autoimmune challenge²³. This could explain the observed diminished tissue inflammation (Fig. 3a, Extended Data Fig. 6a). Accordingly, intrathecal injection of poly I:C, which evokes a type I IFN signature through Toll-like receptor 3 signalling²⁴, significantly interfered with the EAE induction (Fig. 4d). The changed

reactivity of the microglia also became evident after a direct intrathecal stimulation with IFN γ and TNF. In fact, microglial cells from rats that were pre-treated with neomycin showed a reduced activation after a local challenge with these proinflammatory cytokines. Furthermore, the recruitment of inflammatory cells was significantly reduced (Extended Data Fig. 8a). Analyses of in-vitro-stimulated microglia isolated from neomycin-pre-treated or control rats confirmed a reduced reactivity of the microglia after IFN γ stimulation (Extended Data Fig. 8b).

Lipopolysaccharide as a lung microbial CNS regulator

To find out how these alterations in microglial reactivity are linked to the lung microbiome, we next focused on the changes of the lung commensal bacterial communities after intratracheal treatment with neomycin. Gram-negative Bacteroidetes was the most abundant phylum of bacteria (37%), with a 2.5-fold increase in the neomycin-treated group compared to the phosphate-buffered saline (PBS)-treated group (Fig. 5a). In this phylum, the families that showed the greatest increases were the Prevotellaceae, Muribaculaceae and Rikenellaceae, all of which are anaerobes and include members that are resistant to neomycin (Fig. 5b). We also observed an upregulation in other bacterial families, including the Lachnospiraceae and Lactobacillaceae. These qualitative changes in the composition of the lung microbiota were associated with a significant increase in the total bacterial load (Fig. 1a).

We next wanted to find out whether Bacteroidetes—the phylum that was most affected by the neomycin treatment—would be relevant for the observed clinical effects. Therefore, we transferred an inactivated strain from the Bacteroidetes phylum, *Prevotella melaninogenica*. Intratracheal transfer of *P. melaninogenica* led to significantly dampened clinical EAE (Fig. 5c). Transfer of the microbiota by gastrointestinal gavage did not change the disease, which provides further support for the relevance of the lung microbiome in the regulation of the immune reactivity of the CNS (Extended Data Fig. 8c). The efficiency of the metabolically inactive *P. melaninogenica* hints at a structural microbial component, which mediates the immune modulating effects within the CNS. One potential candidate for this is the bacterial cell wall component lipopolysaccharide (LPS), which is well known to evoke type I IFN responses^{25,26}. Considering that Bacteroidetes contribute up to 80% of the LPS production in the gut²⁷, we next quantified the concentration of LPS within the BALF. We observed a significant increase in LPS in neomycin-treated rats (Extended Data Fig. 8d). This increased level of intrapulmonary LPS correlated with an increased type I IFN signature in interstitial macrophages and neutrophils in the lung (Extended Data Fig. 8e). Of note, intratracheal treatment with the antibiotic drug vancomycin—which did not induce a shift towards LPS-producing phyla (Extended Data Fig. 8d, Extended Data Fig. 9a, b)—did not change the microglial expression profile and was not effective in ameliorating EAE (Extended Data Fig. 9c–g). Furthermore, intratracheal application of the LPS-neutralizing antibiotic peptide polymyxin B^{28,29} significantly increased the severity of EAE (Extended Data Fig. 10a). To directly test the role of LPS, we increased its local levels by intratracheal application of LPS from *Escherichia coli* or from *P. melaninogenica*. As was the case with the neomycin treatment or microbiota transfer, LPS supplementation in the lung led to an amelioration of EAE (Fig. 5d, Extended Data Fig. 10b). LPS has been reported to penetrate the BBB and to evoke functional changes in microglia^{30,31}. Therefore, we finally applied LPS directly into the CNS. Intrathecal injection of LPS evoked clear disease-dampening effects that exceeded even those observed after intratracheal LPS applications (Fig. 5e, Extended Data Fig. 9c). The data therefore support the view that a shift towards LPS-producing phyla induces a type I IFN response in the CNS, and that this mechanism underlies the resistance against autoimmune processes (Extended Data Fig. 9d).

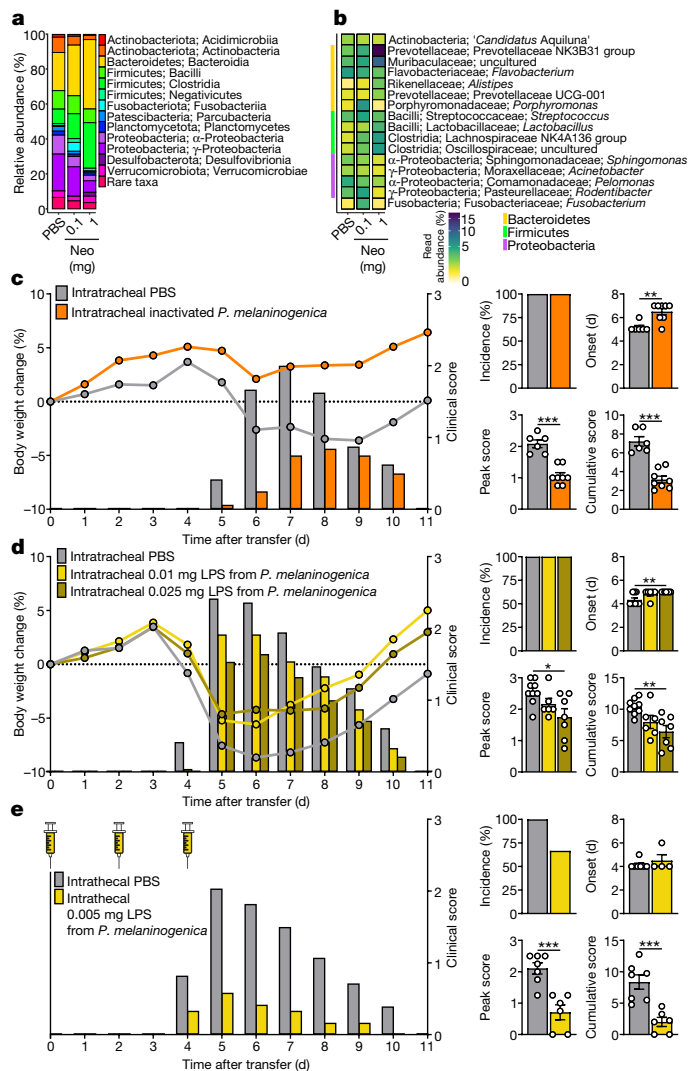


Fig. 5 | Pulmonary LPS controls CNS autoimmunity. **a, b**, Neomycin induces a shift towards LPS-producing phyla in the lung microbiota. **a**, Average relative abundance of bacterial phyla of the lung microbiota in PBS- or neomycin-treated rats. **b**, Corresponding heat map depicting the relative abundance of lung bacterial inhabitants at the family level. **c**, Intratracheal administration of inactivated *P. melaninogenica* has an EAE-suppressive effect. EAE was induced by transfer of T_{MBP} cells. Clinical parameters after daily intratracheal treatment started 7 days before T_{MBP} cell transfer and continued throughout the entire disease course. Mean \pm s.e.m. Cumulative data from two independent experiments. $n = 6$ (PBS); $n = 8$ (*P. melaninogenica*). **d**, Intratracheal treatment with LPS from *P. melaninogenica* ameliorates EAE. Transfer EAE was induced in rats that were pre-treated intratracheally for 7 days with PBS or LPS at the indicated concentration. The treatment was continued throughout the entire disease course. Clinical parameters. Mean \pm s.e.m. Cumulative data from two independent experiments. $n = 9$ (PBS); $n = 6$ (0.01 mg LPS), $n = 7$ (0.025 mg LPS). **e**, Intratracheal administration of LPS from *P. melaninogenica* has a disease-suppressive effect. LPS (0.005 mg per rat) was administered on days 0, 2 and 4 after T_{MBP} cell transfer. Clinical parameters. Mean \pm s.e.m. Cumulative data from two independent experiments. $n = 7$ (PBS); $n = 6$ (LPS). **c, e**, Statistical significance by unpaired two-tailed *t*-test (Gaussian distribution) and Mann-Whitney test (non-Gaussian distribution). **d**, Statistical significance by one-way ANOVA with Tukey's multiple comparisons test. * $P < 0.05$, ** $P < 0.01$, *** $P < 0.001$.

Discussion

Our study indicates a new functional connection between the lung and the brain. This connection is controlled by the local lung microbiota, which apparently continuously sends signals to the microglia, the

'immune cells' of the brain¹⁹. The microglial cells adapt their immunological responsiveness according to these microbial signals. The lung is the most extended body surface³² that is in contact with the outside environment, and it is therefore constantly exposed to microorganisms and contaminants. These pathogens can also pose a danger to the CNS. The pulmonary microbiome, which is directly located at the interface with the outside environment and which in its nature is tailored to react to these external threats, can therefore act as a kind of remote warning system for the sensitive CNS.

Until now, the gut microbiome has had the main focus of attention as a regulator of CNS immune functions³³. There are, however, clear differences in the location and the nature of the microbial signals that are responsible for this regulation. Although remote effects of the gut microbiome on the CNS have been postulated^{8,34,35}, the major focus is on effects in the intestinal milieu, immune structures in the intestine and the draining lymph nodes. Microbial antigens that resemble those of CNS structures could have a role as the initial trigger of the pathogenic T cell response⁹. Conversely, a regulatory function of microbial factors such as polysaccharide A has been discussed³⁶. Furthermore, microbial nutrients or their derivatives, such as short-chained fatty acids or tryptophan metabolites, can influence the activation and differentiation of pathogenic T cells^{37,38}. Although a contribution by microbial metabolites cannot be ruled out in the effects on CNS autoimmunity observed here, our data favour LPS as the trigger of a type I IFN response that interferes with the autoimmune process in EAE models and multiple sclerosis^{23,39,40}. Perhaps the most prominent difference between the gut and the lung microbiome is the extent of manipulation that is necessary to change the immunological situation. Influencing CNS autoimmunity via the gut requires strong interference with the gut microbiome—for example, a high-dosed combined antibiotic that almost completely depletes the microbiota, or housing the animals in a sterile environment. The effects of such interference are strong and range from an atrophy of secondary immune organs to massive local problems (for example, the development of a megacolon)^{34,41–43}. In the lung, by contrast, minimal manipulations—here only a moderate shift in the bacterial diversity—are enough to achieve a corresponding microglial reaction. The pulmonary microbiome is distinct and comprises only a quantitatively tiny population in comparison to that of the gut (at least 10^8 in magnitude)⁴⁴. Therefore, minimal outside influences may suffice to unbalance it. Furthermore, the particularities of the blood–air barrier and the special integration of the lung in the circulatory system can come into play. Thus, the distance to be covered by microbial signal substances to reach the blood is likely to be much shorter for the pulmonary commensals than for the intestinal commensals. Especially in the alveolar area, this distance for the purpose of optimized oxygen exchange is minimized: the border of the cell layers of alveolar cells and capillary endothelium consists only of a shared basement membrane. Moreover, the direct blood flow out of the lung into the arterial system provides unfiltered access to the CNS. The gut has the liver as a 'firewall' between itself and the CNS⁴⁵.

In conclusion, we show here that a well-balanced equilibrium of the pulmonary microbiota tunes the activation state of microglia, most likely through incremented colonization of LPS-producing bacterial taxa. This observation could be of importance in a clinical perspective: infections of the lung, smoking, therapeutic manipulations and environmental factors can all act on the pulmonary microbiome and thus might influence the immune reactivity of the brain. This tight interconnection could potentially be therapeutically exploited, for example, by the local application of probiotics or certain antibiotics. A targeted manipulation of the immune reactivity of the CNS could provide a treatment option not only in an autoimmune situation, but also in a wide range of CNS diseases in which the reactivity of the brain's innate immune response is involved—for example, in infectious or degenerative disorders.

Online content

Any methods, additional references, Nature Research reporting summaries, source data, extended data, supplementary information, acknowledgements, peer review information; details of author contributions and competing interests; and statements of data and code availability are available at <https://doi.org/10.1038/s41586-022-04427-4>.

1. Olsson, T., Barcellos, L. F. & Alfredsson, L. Interactions between genetic, lifestyle and environmental risk factors for multiple sclerosis. *Nat. Rev. Neurol.* **13**, 25–36 (2017).
2. Odoardi, F. et al. T cells become licensed in the lung to enter the central nervous system. *Nature* **488**, 675–679 (2012).
3. O'Dwyer, D. N., Dickson, R. P. & Moore, B. B. The lung microbiome, immunity, and the pathogenesis of chronic lung disease. *J. Immunol.* **196**, 4839–4847 (2016).
4. Jin, C. et al. Commensal microbiota promote lung cancer development via $\gamma\delta$ T cells. *Cell* **176**, 998–1013 (2019).
5. Yokote, H. et al. NKT cell-dependent amelioration of a mouse model of multiple sclerosis by altering gut flora. *Am. J. Pathol.* **173**, 1714–1723 (2008).
6. Ochoa-Repáraz, J. et al. Role of gut commensal microflora in the development of experimental autoimmune encephalomyelitis. *J. Immunol.* **183**, 6041–6050 (2009).
7. Berer, K. et al. Commensal microbiota and myelin autoantigen cooperate to trigger autoimmune demyelination. *Nature* **479**, 538–541 (2011).
8. Rothhammer, V. et al. Type I interferons and microbial metabolites of tryptophan modulate astrocyte activity and central nervous system inflammation via the aryl hydrocarbon receptor. *Nat. Med.* **22**, 586–597 (2016).
9. Miyauchi, E. et al. Gut microorganisms act together to exacerbate inflammation in spinal cords. *Nature* **585**, 102–106 (2020).
10. Flügel, A., Willem, M., Berkowicz, T. & Wekerle, H. Gene transfer into CD4⁺ T lymphocytes: green fluorescent protein-engineered, encephalitogenic T cells illuminate brain autoimmune responses. *Nat. Med.* **5**, 843–847 (1999).
11. Lodygin, D. et al. β -Synuclein-reactive T cells induce autoimmune CNS grey matter degeneration. *Nature* **566**, 503–508 (2019).
12. Bartholomäus, I. et al. Effector T cell interactions with meningeal vascular structures in nascent autoimmune CNS lesions. *Nature* **462**, 94–98 (2009).
13. Kivisäkk, P. et al. Localizing central nervous system immune surveillance: meningeal antigen-presenting cells activate T cells during experimental autoimmune encephalomyelitis. *Ann. Neurol.* **65**, 457–469 (2009).
14. Lodygin, D. et al. A combination of fluorescent NFAT and H2B sensors uncovers dynamics of T cell activation in real time during CNS autoimmunity. *Nat. Med.* **19**, 784–790 (2013).
15. Starossom, S. C. et al. Galectin-1 deactivates classically activated microglia and protects from inflammation-induced neurodegeneration. *Immunity* **37**, 249–263 (2012).
16. Kawakami, N. et al. The activation status of neuroantigen-specific T cells in the target organ determines the clinical outcome of autoimmune encephalomyelitis. *J. Exp. Med.* **199**, 185–197 (2004).
17. Odoardi, F. et al. Instant effect of soluble antigen on effector T cells in peripheral immune organs during immunotherapy of autoimmune encephalomyelitis. *Proc. Natl Acad. Sci. USA* **104**, 920–925 (2007).
18. Heppner, F. L. et al. Experimental autoimmune encephalomyelitis repressed by microglial paralysis. *Nat. Med.* **11**, 146–152 (2005).
19. Hanisch, U. K. & Kettenmann, H. Microglia: active sensor and versatile effector cells in the normal and pathologic brain. *Nat. Neurosci.* **10**, 1387–1394 (2007).
20. Rock, R. B. et al. Transcriptional response of human microglial cells to interferon- γ . *Genes Immun.* **6**, 712–719 (2005).
21. Popovic, N. et al. Inhibition of autoimmune encephalomyelitis by a tetracycline. *Ann. Neurol.* **51**, 215–223 (2002).
22. Elmore, M. R. et al. Colony-stimulating factor 1 receptor signaling is necessary for microglia viability, unmasking a microglia progenitor cell in the adult brain. *Neuron* **82**, 380–397 (2014).
23. Prinz, M. et al. Distinct and nonredundant in vivo functions of IFNAR on myeloid cells limit autoimmunity in the central nervous system. *Immunity* **28**, 675–686 (2008).
24. Khorrooshi, R. et al. Induction of endogenous type I interferon within the central nervous system plays a protective role in experimental autoimmune encephalomyelitis. *Acta Neuropathol.* **130**, 107–118 (2015).
25. McNab, F., Mayer-Barber, K., Sher, A., Wack, A. & O'Garra, A. Type I interferons in infectious disease. *Nat. Rev. Immunol.* **15**, 87–103 (2015).
26. Bradley, K. C. et al. Microbiota-driven tonic interferon signals in lung stromal cells protect from influenza virus infection. *Cell Rep.* **28**, 245–256 (2019).
27. d'Hennezel, E., Abubucker, S., Murphy, L. O. & Cullen, T. W. Total lipopolysaccharide from the human gut microbiome silences toll-like receptor signaling. *mSystems* **2**, e00046-17 (2017).
28. Yang, D. et al. Dysregulated lung commensal bacteria drive interleukin-17B production to promote pulmonary fibrosis through their outer membrane vesicles. *Immunity* **50**, 692–706 (2019).
29. Bhor, V. M., Thomas, C. J., Suroliya, N. & Suroliya, A. Polymyxin B: an ode to an old antidote for endotoxin shock. *Mol. Biosyst.* **1**, 213–222 (2005).
30. Vargas-Caraveo, A. et al. Lipopolysaccharide enters the rat brain by a lipoprotein-mediated transport mechanism in physiological conditions. *Sci. Rep.* **7**, 13113 (2017).
31. Sandiego, C. M. et al. Imaging robust microglial activation after lipopolysaccharide administration in humans with PET. *Proc. Natl Acad. Sci. USA* **112**, 12468–12473 (2015).
32. Dickson, R. P., Erb-Downward, J. R., Martinez, F. J. & Huffnagle, G. B. The microbiome and the respiratory tract. *Annu. Rev. Physiol.* **78**, 481–504 (2016).
33. Belkaid, Y. & Hand, T. W. Role of the microbiota in immunity and inflammation. *Cell* **157**, 121–141 (2014).
34. Erny, D. et al. Host microbiota constantly control maturation and function of microglia in the CNS. *Nat. Neurosci.* **18**, 965–977 (2015).
35. Braniste, V. et al. The gut microbiota influences blood–brain barrier permeability in mice. *Sci. Transl. Med.* **6**, 263ra158 (2014).
36. Wang, Y. et al. An intestinal commensal symbiosis factor controls neuroinflammation via TLR2-mediated CD39 signalling. *Nat. Commun.* **5**, 4432 (2014).
37. Luu, M. et al. The short-chain fatty acid pentanoate suppresses autoimmunity by modulating the metabolic-epigenetic crosstalk in lymphocytes. *Nat. Commun.* **10**, 760 (2019).
38. Sonner, J. K. et al. Dietary tryptophan links encephalogenicity of autoreactive T cells with gut microbial ecology. *Nat. Commun.* **10**, 4877 (2019).
39. Jakimovski, D., Kolb, C., Ramanathan, M., Zivadinov, R. & Weinstock-Guttman, B. Interferon β for multiple sclerosis. *Cold Spring Harb. Perspect. Med.* **8**, a032003 (2018).
40. Guo, B., Chang, E. Y. & Cheng, G. The type I IFN induction pathway constrains Th17-mediated autoimmune inflammation in mice. *J. Clin. Invest.* **118**, 1680–1690 (2008).
41. Bauer, H., Horowitz, R. E., Levenson, S. M. & Popper, H. The response of the lymphatic tissue to the microbial flora. Studies on germfree mice. *Am. J. Pathol.* **42**, 471–483 (1963).
42. Smith, K., McCoy, K. D. & Macpherson, A. J. Use of axenic animals in studying the adaptation of mammals to their commensal intestinal microbiota. *Semin. Immunol.* **19**, 59–69 (2007).
43. Kennedy, E. A., King, K. Y. & Baldrige, M. T. Mouse microbiota models: comparing germ-free mice and antibiotics treatment as tools for modifying gut bacteria. *Front. Physiol.* **9**, 1534 (2018).
44. Wypych, T. P., Wickramasinghe, L. C. & Marsland, B. J. The influence of the microbiome on respiratory health. *Nat. Immunol.* **20**, 1279–1290 (2019).
45. Balmer, M. L. et al. The liver may act as a firewall mediating mutualism between the host and its gut commensal microbiota. *Sci. Transl. Med.* **6**, 237ra266 (2014).

Publisher's note Springer Nature remains neutral with regard to jurisdictional claims in published maps and institutional affiliations.

© The Author(s), under exclusive licence to Springer Nature Limited 2022

Methods

Rats

Male and female 6–10-week-old wild type and bSYN TCR-transgenic rats¹¹ on a LEW/Crl (*Rattus norvegicus*) background were used for all experiments and for the generation of T cell lines. The rats were kept in GR9000 IVC cages at a 12–12-h light–dark cycle with food and water provided ad libitum. They were bred and raised at the animal facilities of the University Medical Center Göttingen. All experiments were performed in accordance with the regulations of animal welfare of Lower Saxony, Germany. No differences were noted between the sexes.

Antigens

Myelin basic protein (MBP) was extracted from guinea pig brain as previously described⁴⁶, β -synuclein_{93–111} peptide (bSYN) was synthesized by the peptide facility of the Charité (Berlin), and ovalbumin (OVA) was purchased from Sigma-Aldrich.

Generation and culturing of T cells

CD4⁺ T cells retrovirally transduced to express Life-act Turquoise (CFP) or eGFP (GFP) and reactive against MBP (T_{MBP}), bSYN (T_{bSYN}) or OVA (T_{OVA}) were generated as previously reported^{10,11}. In brief, female Lewis rats were immunized subcutaneously at the tail base (s.c.) with 150 μ l of an emulsion consisting of equal parts of antigen (MBP, bSYN or OVA; 1 mg ml⁻¹) and complete Freund's adjuvant (CFA, Difco) containing *Mycobacterium tuberculosis H37Ra* extract (2 mg ml⁻¹, BD). Nine to ten days after immunization, the cell suspension obtained from the draining lymph nodes was co-cultured with GP+E86 packaging cell lines producing replication-deficient retroviruses expressing a fluorescent protein of interest and an antibiotic-resistant gene in the presence of MBP (10 μ g ml⁻¹), OVA (10 μ g ml⁻¹) or bSYN (8 μ g ml⁻¹) in DMEM-based medium containing 1% rat serum. Forty-eight hours later, T cells were expanded by adding DMEM-based medium containing horse serum (10%, Biochrom AG) and mouse IL-2. Starting from day 4 after antigen stimulation, transduced T cells were selected by the addition of G418 (400 mg ml⁻¹, Thermo Fisher Scientific) for two weeks or puromycin (1 μ g ml⁻¹, Carl Roth) for one week. On day 7 after primary stimulation, 3.5 \times 10⁶ T cells were challenged with the cognate antigen in the presence of 70 \times 10⁶ irradiated thymic APCs. The primary cell lines underwent at least three cycles of stimulation in culture before being used for transfer experiments. All established T cell lines were $\alpha\beta$ TCR⁺ CD4⁺ CD8⁻ and had an effector memory phenotype (L-selectin⁻, CD45RC^{low} and CD44^{high}). Upon stimulation, they produced IFN γ and IL-17. Phenotype, cytokine profile, antigen specificity, pathogenicity and the absence of mycoplasma contamination were verified in each cell line.

EAE models and scoring system

Adoptive transfer EAE and T-cell-mediated grey matter disease.

Fully activated T_{MBP} or T_{bSYN} cell blasts (day 2 after antigen encounter) were injected in the tail vein of recipient wild-type rats in EH medium. If not stated otherwise, 2.5 \times 10⁵ T_{MBP} cell blasts or 1.5 \times 10⁶ T_{bSYN} cell blasts per rat were transferred. As a control, 2.5 \times 10⁵ T_{OVA} cell blasts were intravenously injected following the same procedure.

Lung EAE. Resting T_{MBP} cells (7.5 \times 10⁶, day 6 after antigen encounter) in EH medium were injected into the tail vein of recipient wild-type rats. Six hours later the rats were immunized intratracheally. For this purpose, rats were briefly anaesthetized with ether and fixed with a bar behind their upper incisors on a stand in an upright position slightly leaning backwards. The trachea was located using a Small Animal Laryngoscope LS-2 (Penn Century). Subsequently, an emulsion consisting of equal parts of antigen, that is, MBP or OVA (0.02 mg ml⁻¹), and CFA (0.2 mg ml⁻¹) was instilled into the trachea through a winged 18G catheter (B. Braun). Each rat received a total volume (in μ l) corresponding to around one-third of its body weight (in g). The rats were then released

from the stand and transferred to their cages to recover. The entire procedure typically lasted approximately 1 min per rat.

Subcutaneous EAE. Resting T_{MBP} cells (7.5 \times 10⁶, day 6 after antigen encounter) in EH medium were injected into the tail vein of recipient wild-type rats. Six hours later, an emulsion consisting of equal parts of antigen, that is, MBP or OVA (1 mg ml⁻¹), and CFA (1 mg ml⁻¹) was injected subcutaneously (s.c.) into the popliteal cavities of both hind limbs of ether-anaesthetized rats. Each rat received a total volume (in μ l) corresponding to around one-third of its body weight (in g).

EAE scoring. Weight and clinical scores were recorded daily. Classical signs of EAE were scored as follows: 0 = no disease; 1 = flaccid tail; 2 = gait disturbance; 3 = complete hind limb paralysis; 4 = tetraparesis; 5 = death. For atypical symptoms that could occur after transfer of T_{bSYN} cells, the following classification was used: 0 = no disease; 1 = occasional twitches and scratching with or without flaccid tail; 2 = frequent twitches and scratching, ataxia; 3 = severe tonic and myoclonic movements, severe gait impairment; 4 = tetraparesis; 5 = death. Rats with a clinical score above 3 were euthanized.

No statistical methods were used to predetermine sample size. Clinical score was assessed in a blinded fashion. Rats were randomly allocated to experimental groups.

Antibiotic treatment

Neomycin (Thermo Fisher Scientific) or vancomycin (Abcam) were administered intratracheally (daily dose: 0.1 or 1 mg; volume: 150 μ l), subcutaneously into the popliteal cavity (daily dose: 1 mg; volume: 50 μ l) or orally by gavage (daily dose: 1 or 10 mg; volume: 300 μ l). The intratracheal dose of antibiotics was selected after initial titration on the basis that it did not change the immune cell composition of the lung. Polymyxin B (Roth) was administered intratracheally (daily dose: 0.1 mg; volume: 150 μ l). The antibiotics were freshly prepared before every treatment by dissolving the powder in sterile PBS. An equivalent volume of PBS was used as control. If not stated otherwise, neomycin and vancomycin were administered at a daily dose of 1 mg per rat. The rats were treated daily for 7 days before starting the experiment. Daily treatment was continued throughout the entire experiment. Of note, both the intratracheal and the oral antibiotic treatments were well tolerated by the rats. No respiratory distress or diarrhoea were observed and the rats steadily increased their body weight comparably to the controls.

Transfer of BALF-derived microbiota

Rats were intratracheally treated with neomycin. After 7 days, the treatment was stopped and the rats were intratracheally transferred with BALF-derived microbiota of rats that were intratracheally pre-treated for 7 days with either PBS or neomycin (donor group). Immediately after the microbiota transfer, EAE was induced by intravenous injection of T_{MBP} cells. The treatment with BALF-derived microbiota was performed daily for the entire disease course.

For the collection of microbiota, sterile BALF (8 ml per rat) was collected daily from either the PBS- or the neomycin-donor group as described in 'Collection of BALF and faecal samples'. The BALF was centrifuged for 10 min at 13,000 rpm and 4 °C and the bacterial pellet was resuspended in 450 μ l sterile PBS. Each rat of the recipient group received a daily dose of 150 μ l of the corresponding BALF resuspension.

Functional inhibition of microglia by minocycline treatment

PBS-treated or neomycin-treated rats received intraperitoneal minocycline hydrochloride (Sigma-Aldrich) dissolved in 40% 2-hydroxypropyl- β -cyclodextrin (vehicle; ITW Reagents; daily dose: 50 mg per kg rat body weight). Injection of the same volume of vehicle served as control. Treatments with PBS/neomycin and minocycline/vehicle started 7 days before T_{MBP} cell transfer and were continued throughout the entire EAE course. Of note, the intraperitoneal treatment was

Article

well-tolerated by the rats. No distress was observed and the rats steadily increased their body weight comparably to the controls.

Depletion of microglia by PLX3397 treatment

PBS-treated or neomycin-treated rats received the CSF1R inhibitor PLX3397 (MedChemExpress) dissolved in 0.5% HPMC/1% Tween80/2.5% DMSO (daily dose: 30 mg per kg rat body weight) or vehicle by gavage. Treatments with PBS/neomycin and PLX3397/vehicle started 7 days before T_{MBP} cell transfer and were continued throughout the entire EAE course. Of note, the oral treatment was well tolerated by the rats. No distress was observed and the rats steadily increased their body weight comparably to the controls.

Treatments with poly I:C, inactive *Prevotella melaninogenica* and LPS

Poly I:C treatment. Polyinosinic-polycytidylic acid sodium salt (poly I:C; Sigma-Aldrich) was dissolved in sterile water at a stock concentration of 10 mg ml⁻¹. Aliquots were stored at -20 °C and thawed shortly before injection. Poly I:C solution (1 mg in 100 µl) was administered intrathecally in rats anaesthetized with ketamine (50 mg per kg; Medistar) and xylazine (10 mg per kg; Ecuphar). Half of the dose (50 µl) was injected into the cisterna magna and the remaining half into the lumbar spinal cord (L4–L5) using a stereotactic device (Narishige). The treatment was performed on days 0, 2 and 4 after T_{MBP} cell transfer. Sterile PBS was used as control. Of note, 24 h after intrathecal injection, the rats showed a reduction in body weight as reported⁴⁷. As this symptom occurred independently of EAE symptoms, body weight changes are not depicted in the corresponding graphs.

Treatment with inactive *Prevotella melaninogenica*. *Prevotella melaninogenica* (*P. melaninogenica*; type strain DSM 7089; DSMZ) was grown anaerobically in modified PYG medium (Medium 104; DSMZ) at 37 °C. For transfer experiments of inactive *P. melaninogenica*, the culture was grown to a concentration of 30 × 10⁶ colony-forming units (CFU) per ml. The culture was chemically inactivated using chicken egg lysozyme (2 mg l⁻¹; SERVA) and subsequently heat-inactivated at 99 °C for 30 min. Successful inactivation was verified by the inability of the bacteria to regrow in culture. Before transfer, the samples were centrifuged at 13,000 rpm for 10 min at 4 °C and resuspended in sterile PBS. Rats received daily 5 × 10⁵ CFU in 150 µl sterile PBS daily or 150 µl sterile PBS as control either intratracheally or orally. The treatment was started 7 days before disease induction by transfer of T_{MBP} cells and continued throughout the entire experiment.

***Prevotella melaninogenica* LPS treatment.** For LPS extraction, *P. melaninogenica* was cultured as described in 'Treatment with inactive *Prevotella melaninogenica*'. The culture was grown to an optical density at 600 nm (OD₆₀₀) of 0.8–1.2. LPS was extracted using a LPS Extraction Kit (iNtRON) according to the manufacturer's instructions. The yield was quantified using the Pierce Chromogenic Endotoxin Quant Kit (Thermo Fisher Scientific). *E. coli* LPS (serotype O127: B8; Sigma-Aldrich) served as an additional control.

Solution with LPS from *P. melaninogenica* was freshly prepared before every treatment by dissolving the isolated LPS pellet in sterile PBS by boiling the vial for 5 min. *P. melaninogenica* LPS was administered intratracheally (dose: 0.01 or 0.025 mg in 150 µl PBS) or intrathecally (dose: 0.005 mg in 30 µl PBS). For the intratracheal treatment, LPS was administered daily starting on day 7 before disease induction by transfer of T_{MBP} cells and continued throughout the entire experiment. For intrathecal treatment, *P. melaninogenica* LPS was injected as above in the cisterna magna on days 0, 2 and 4 after T_{MBP} cell transfer. Sterile PBS was used as control.

***Escherichia coli* LPS treatment.** *Escherichia coli* (*E. coli*; serotype O127: B8; Sigma-Aldrich) was administered intratracheally (0.01 mg

in 150 µl PBS) or intrathecally (0.003 mg in 30 µl PBS) following the same schedule as for *P. melaninogenica* LPS treatments. The daily intratracheal LPS dose was 50 times lower than the dose administered in a model of acute lung injury⁴⁸ and was well-tolerated by the rats. No respiratory distress was observed and the rats steadily increased their body weight comparably to the controls. After intrathecal treatments with either *P. melaninogenica* or *E. coli* LPS, as observed with poly I:C administration, the rats displayed a reduction in body weight not related to EAE. Therefore, body weight changes are not depicted in the corresponding graphs.

Lung and gut microbiota analysis

Description of the samples. For characterizing the changes of lung and gut microbiota after intratracheal antibiotic treatment, BALF and faeces samples were collected from rats that were daily treated with neomycin (0.1 or 1 mg per day), vancomycin (0.1 or 1 mg per day) or PBS for 7 days. For each cohort, six samples from two independent experiments each including three rats per group per treatment were analysed. For characterizing the changes in gut microbiota after oral antibiotic treatment, faecal samples were collected from rats that were daily treated with neomycin (1 or 10 mg per day) or PBS for 7 days. For each cohort, six samples from two independent experiments each including three rats per group per treatment were analysed.

Collection of BALF and faecal samples. BALF and faecal samples were collected under sterile conditions from the same rats. In brief, the rats were euthanized using an overdose of ketamine/xylazine. After carefully disinfecting the rat's fur with 70% ethanol, a tracheotomy was performed and a sterile gavage needle (18G) was inserted into the trachea under a laminar flow hood. The gavage needle was fixed and held in position using a surgical suture (B. Braun). Five millilitres of pre-warmed (37 °C) PBS was slowly instilled into the lung and after 30 s a volume of 4 ml was retrieved. This step was repeated once, yielding 8 ml of total BALF per rat. Faecal samples were collected from the recto-anal region. BALF (in 2-ml aliquots) and faecal samples were immediately snap-frozen on dry ice and stored at -80 °C until further processing.

Lysis and nucleic acid extraction. To efficiently extract nucleic acids from both gram-positive and gram-negative bacteria, a pre-lysis step was performed by incubating 400 µl BALF with 2 µl chicken egg lysozyme (100 mg ml⁻¹; SERVA) at 37 °C and 180 rpm for 1 h. DNA extraction from BALF was performed using the QIAamp cador Pathogen Mini Kit (Indical Bioscience) according to the manufacturer's instructions. DNA was eluted with 50 µl sterile water. Rat faecal samples (around 150 mg) were resuspended in 1 ml InhibitEX buffer (Qiagen) at 37 °C for 15 min for homogenization and mixed every 5 min with an inoculation loop. Faecal sample DNA was extracted using the QIAamp Fast DNA Stool Mini Kit (Qiagen) according to the manufacturer's instructions. DNA was eluted with 200 µl sterile water. Extracted nucleic acids were quality-checked using 0.8% LE Agarose (Biozym) gel electrophoresis. Nucleic acid concentrations were quantified using a NanoDrop ND-1000 Spectrophotometer (Thermo Fisher Scientific).

Quantification of bacterial number. The bacterial load of rat BALF and faecal samples was estimated by analysing the expression of the protein elongation factor Tu (*tuf*) gene by quantitative PCR using the Bacteria (*tuf* gene) Quantitative PCR Kit (Takara) and an iQ5 Multicolor Real-Time PCR Detection System (BioRad). PCR and cycling conditions were set according to the manufacturer's instructions. All samples were prepared at least in duplicate. CT values of the individual measurements did not exceed 1.5 amplification cycles. For the BALF samples, the copy number of the *tuf* gene was normalized to 100 µl for each sample. Faecal samples were normalized on the basis of the weighed amount used for DNA extraction. The copy number of the *tuf* gene was finally normalized for 100 µg of faeces for each sample.

16S amplicon generation and sequencing. Bacterial 16S rRNA amplicons were generated using Klindworth primers with adapters for Illumina MiSeq sequencing targeting the V3–V4 region⁴⁹. For BALF samples, PCR mixtures (50 μ l) contained 1 \times Phusion GC buffer (5 \times), 0.2 mM of each deoxynucleoside triphosphate, 5% DMSO, 0.1 mM MgCl₂, 0.2 μ M of each primer and 0.02 U of Phusion High-Fidelity DNA Polymerase (Thermo Fisher Scientific). As template, approximately 150 or 350 ng of isolated BALF or faecal DNA, respectively, was used. Negative and positive controls contained no DNA template or genomic *Bacillus* DNA, respectively. For amplicon amplification of BALF samples, the following cycler program was used: initial denaturation at 98 °C for 1 min, 35 cycles of denaturation at 98 °C for 45 s, annealing at 62 °C for 45 s and extension at 72 °C for 45 s, followed by a final extension at 72 °C for 5 min. For faecal samples, the 25 PCR cycles were performed with an extension time of 30 s. Each PCR reaction was performed in triplicate. The resulting PCR products were pooled in equal amounts and purified with the MagSi-NGSPrep Plus Kit (Steinbrenner) according to the manufacturer's instructions. Amplicons were eluted in 40 μ l sterile water and quantified with the Quant-iT dsDNA HS assay kit and a Qubit fluorometer (Invitrogen). The indexing of the amplicons was performed with the Nextera XT Index-Kit (Illumina). The 16S rRNA gene sequencing was performed using the dual index paired-end approach (2 \times 300 bp) with v3 chemistry for the Illumina MiSeq platform.

Processing of 16S rRNA sequencing data. Raw sequencing data were initially processed using the Miseq marker gene pipeline v.1.8⁵⁰. Further processing was performed using VSEARCH v.2.12.06⁵¹ and the UNOISE3 algorithm. Raw sequencing reads were mapped to the amplicon sequence variant (ASV) table. The similarity threshold was set at 100%. Taxonomic classification of ASVs was performed using BLASTn 2.7.1 against the SILVA SSU NR database release 138^{52,53}. If not otherwise stated, all bioinformatic tools were used with default parameters.

Statistical analyses. Subsampling, removal of chloroplasts, eukaryote, mitochondria, archaea and unclassified ASVs, as well as statistical analysis including diversity analysis and visualization, was performed in Rstudio v.1.3.1056 (RStudio Team, 2020) and R 4.0 (R Core Team, 2013). Inter-sample data normalization was performed in R using the geometric mean of pairwise ratios package (GMRP v.0.1.3)⁵⁴. Data were visualized using ampvis2 (v.2.6.4)⁵⁵ and the implemented package ggplot2 (v.3.3.2)⁵⁶. Alpha-diversity metrics and species richness were used to characterize the bacterial diversity within each sample, which included calculation of the Shannon diversity index and phylogenetic diversity index. All samples were rarefied in ampvis2 to the corresponding lowest number of reads per treatment. The normality of data distribution was examined by the Shapiro–Wilk test. ANOVA was used to compare parametric variables among three or more groups, and the Kruskal–Wallis test was used for non-parametric variables. To compare means between unpaired groups with an assumption of unequal variance between sample sets, the independent *t*-test was used, and for non-parametric variables the Mann–Whitney *U*-test. *P* values less than 0.05 were considered to indicate statistical significance. For visualization in bar charts, the mean of treatment replicates was used to account for the variance in animal samples. To visualize the multivariate dispersion of the composition of the community, the non-metric multidimensional scaling (NMDS) matrix of the Bray–Curtis dissimilarity between samples was calculated by the ampvis2 package (v.2.6.4) wrapping around the vegan package (v.2.5-6) using the ASV table and the phylogenetic tree. Ordination plots were created with ggplot2 (3.3.2) with bray as distance measure. For heat maps the amp_heat function implemented in ampvis2⁵⁵ was used to identify the most abundant taxa (mean) in different treatments and antibiotic concentration. Taxonomic classification is indicated on the class and genus level.

Quantitative analysis of LPS

The amount of LPS in BALF samples was measured in triplicates using the Pierce Chromogenic Endotoxin Quant Kit (Thermo Fisher Scientific) according to the manufacturer's instructions. Values are expressed in international endotoxin units (EU) per ml.

Cell isolation

Rats were intracardially perfused for 6 min with PBS before organ explant. Mononuclear cells were isolated as previously described^{2,10} and kept on ice in EH medium until processed. The procedures are briefly summarized below: EDTA-treated blood was retrieved from the heart by cardiac puncture. Mononuclear cells were isolated by density gradient using Lymphocyte Separation Medium (PromoCell; centrifugation settings: 30 min at 840g and 20 °C). Lungs were thoroughly and repeatedly sectioned using a tissue chopper (McIlwain). The homogenized tissue was washed with EH. Pellets were resuspended and incubated with 2 ml of 0.3% collagenase in PBS for 30 min at 37 °C under constant shaking. Subsequently, the tissue was homogenized using a gentleMACS Dissociator (Miltenyi Biotec), forced through a cell strainer (40 μ m) and washed with EH. The pellet was resuspended in 5 ml 40% isotonic Percoll and underlaid with 5 ml 70% Percoll (centrifugation settings: 30 min at 2,000 rpm and 4 °C). The leukocyte-enriched interphase was then collected, washed and resuspended in EH medium. Spleens and lymph nodes were passed through a cell strainer (40 μ m), washed once with PBS and treated with ACK-buffer for erythrocyte lysis. Parenchyma and leptomeninges of brain and spinal cord were passed through a cell strainer (40 μ m) and washed once with PBS. Myelin debris was eliminated by Percoll-density gradient (centrifugation settings: 30 min at 700g and 4 °C). For endothelial cell isolation, spinal cords were dissected, and the meninges were removed from the parenchyma. Spinal cord parenchyma was brought to single cell suspension using a Dounce homogenizer. The meninges were chopped up using a razor blade. The CNS tissues were then digested with liberase (0.4 U ml⁻¹; Roche) and DNase I (120 U ml⁻¹; Roche) at 37 °C for 1 h with gentle pipetting of the solution every 10 min. Subsequently, the cell suspension was passed through a 40- μ m cell strainer. Myelin debris was removed using a Percoll-density gradient as described above. After washing, the pellets were antibody-labelled in staining-buffer and sorted by fluorescence-activated cell sorting (FACS) as described below.

Flow cytometry and FACS

Flow cytometry analysis was performed with a FACSCalibur operated by Cell Quest software (Becton Dickinson) or with a CytoFLEX flow cytometer operated with CytExpert software (Beckmann Coulter).

The following anti-rat monoclonal antibodies were used for surface staining: α BTcr-AF647 (clone R73, Biolegend), CD45RA-PE (clone OX-33, Biolegend), CD8 α -FITC (OX-8; Biolegend) and CD8 α -PerCP (BD Biosciences), CD4-PE/Cy7 and CD4-PE/Cy5 (Clone W3/25, both BD Biosciences), CD134-BV421 (Clone OX40, BD Biosciences), CD25-PE (Clone OX39, Biolegend), CD62L-PE (clone OX85, Biolegend), LFA-1-APC (integrin α L, clone WT.1, Serotec), VLA-4-APC (anti-CD49d, clone TA-2, Sigma-Aldrich), CD31-PE (clone TLD-3A12, BD Biosciences), CD11b/c-PE and CD11b/c-APC (clone OX-42, Biolegend), CD45-PE, CD45-AF647 and CD45-PerCP (clone OX-1; all Biolegend), GLAST-APC (ACSA1, Miltenyi), RT1B-FITC (clone OX-6, BD Biosciences), RP3-BV421 (BD Biosciences) and CD172a-FITC (Clone ED9, Bio-Rad). Matching directly labelled mouse IgM (clone R6-60.2, BD Biosciences), mouse IgG-APC (Jackson) and mouse IgG1 κ (MOPC 31C, Sigma-Aldrich) were used as isotype controls. Antibodies were used at a concentration of 1:200.

For measuring IFN γ and IL-17 expression, ex-vivo-isolated cells were left unstimulated or stimulated in vitro with 1 μ g ml⁻¹ PMA (Phorbol 12-myriylate 13-acetate, Sigma-Aldrich) and 5 μ M ionomycin calcium salt (Sigma-Aldrich) for 30 min. Brefeldin A (5 μ g ml⁻¹) was added to block cytokine secretion. Cells were cultured for a further

Article

2 h and surface-stained with anti-rat $\alpha\beta$ TCR-AlexaFluor647 (Clone R73, Biolegend), anti-rat CD4-PE/Cy7 (Clone W3/25, Biolegend) and anti-CD8 α -PerCP (Clone OX-8, Biolegend) for 30 min at 4 °C. The cells were fixed with 2% PFA, permeabilized with BD Perm/Wash buffer (BD Biosciences) and stained with rat anti-mouse anti-IL17-BV42 (clone TC11-8H4, Biolegend) and mouse anti-rat IFN γ -PE (Clone DB1, Biolegend) for 45 min at 4 °C. For intracellular staining for FOXP3 detection, ex-vivo-isolated cells were surface-stained as described above, fixed and permeabilized using the Foxp3/transcription factors staining buffer set (eBioscience) following the manufacturer's instructions and stained with anti-mouse/rat/human FOXP3-PE (Biolegend).

For characterization of the expression profile, cells were sorted using a FACS Aria 4L SORP cell sorter (Becton Dickinson) controlled by FACS Diva software (BD) at a low flow rate under constant cooling (4 °C). T_{MBP} cells, endogenous $\alpha\beta$ TCR⁺ CD4⁺ and CD8⁺ T cells, CD45⁺ CD11b⁻ stromal cells, CD45⁺ CD11b⁺ ED9⁻ interstitial macrophages, CD45⁺ CD11b⁺ ED9⁺ alveolar macrophages or recruited monocytes and RP3⁺ neutrophils were sorted from the lung. For obtaining T cells from the lungs for transcriptome analysis, CD11b⁺ cells were depleted before sorting using anti-PE MicroBeads for MACS separation (Miltenyi Biotec) according to the manufacturer's instructions. For characterization of CNS-resident cells in neomycin- versus PBS-treated rats, CD11b⁻ GLAST⁺ astrocytes and CD45^{low} CD11b⁺ microglial cells were sorted. In inflamed conditions, cell characterization was performed on CD45^{low} CD11b⁺ microglial cells and CD45^{high} CD11b⁺ M Φ , which comprise both recruited monocytes and resident macrophages. Of note, even though microglia upregulated CD11b in inflamed conditions, they were still well distinguishable from CD45^{high} CD11b⁺ M Φ (Supplementary Fig. 1). The sorted cells were centrifuged at 1,500g for 4 min at 4 °C and the pellet was resuspended in 300 μ l TRI reagent (Merck) and 1 μ l glycogen (Roche). The samples were stored at -80 °C until further processing. Data analysis was performed with FlowJo LLC (v.10) or CytExpert (5.2) software.

Gating strategies used throughout the manuscript are depicted in Supplementary Fig. 1.

Neomycin toxicity assay

T_{MBP} cells (5×10^4 per well) were challenged with MBP (10 mg ml⁻¹) in the presence of irradiated thymocytes (5×10^5 per well) in 96-well flat bottom plates (Thermo Fisher Scientific). Neomycin was added in various concentrations (100 ng–10 mg ml⁻¹). The cells were incubated at 37 °C and 10% CO₂. T cell proliferation was quantified by flow cytometry on days 2, 3 and 4 after antigen encounter. On day 2, 50 μ l of IL-2-containing growth medium was added to wells acquired on day 3 (and 4). The same procedure was repeated on day 3 for samples acquired on day 4. In addition, after in vitro exposure to neomycin (1 or 10 mg ml⁻¹), 2.5×10^5 T_{MBP} cell blasts (day 2 after stimulation) were adoptively transferred into naive recipient rats and the clinical course of EAE was monitored over the following days.

Intravital TPLSM

TPLSM and spinal cord preparation were performed as described previously^{11,12,57}. The procedures are briefly summarized below. TPLSM was used to image the motility and infiltration of fluorescently labelled T_{MBP} and T_{OVA} cells in the spinal cord of living rats. In addition, the technique was used to analyse BBB permeability. Imaging of T_{MBP} cells was performed in the preclinical phase, at the onset and at the peak of EAE.

Surgical procedures. The rats were pre-anaesthetized with a subcutaneous injection of 75 mg kg⁻¹ ketamine (Medistar) combined with 0.5 mg kg⁻¹ medetomidin (Vetpharm). Subsequently, they were intubated through a small incision of the trachea and immediately ventilated with 1.5–2% of isoflurane (CP-Pharma). During imaging, rats were stabilized in a custom-made microscope stage and their body temperature was regulated and maintained (36–37 °C) by a heated pad connected to a custom-built thermocontroller. Fluid supply during

imaging sessions was maintained using a perfusing device (Ismatec) set to a 0.6 ml h⁻¹ flow rate. Thoracic leptomeninges were accessed as described^{12,57} by performing a laminectomy at level Th12/L1 and carefully removing the dura mater.

Technical equipment and labelling procedures. TPLSM imaging was performed as previously described^{11,12,57} using two different systems: (1) a Zeiss Laser Scanning Microscope 710 (Carl Zeiss) combined with a Coherent 10 W Ti:Sapphire chameleon laser (Coherent), controlled by Zeiss ZEN 2012 SP2 v.2.1 software; and (2) an Olympus FVMPE-RS TPLSM equipped with a Spectra-Physics Mai Tai Ti:Sapphire oscillator and a Mai Tai DeepSee Ti:Sapphire oscillator. The excitation wavelength was tuned to 880 nm or 1,010 nm and routed through a 20 \times water 1.0 NA immersion objective W Plan Apochromat (Carl Zeiss) or a 25 \times water 1.05 NA immersion objective Olympus Scaleview. Excitation at 1,100 nm was propagated by using either a Ti:Sapphire laser pumped OPO in the Zeiss TPLSM or a Mai Tai DeepSee Ti:Sapphire oscillator in the Olympus TPLSM. Emitted fluorescence was detected using non-descanned detectors equipped with 442/46 nm, 483/32 nm and 624/40 nm band-pass filters. Typically, areas of 424.27 μ m \times 424.27 μ m (Zeiss) or 508.93 μ m \times 508.93 μ m (512 \times 512 pixels, Olympus) width were scanned and 50–100- μ m z-stacks were acquired. For overviews, several tile scans were acquired sequentially and stitched together. For reproducible motility analyses, the interval time was kept at 30 s for the Zeiss TPLSM and 15 s for the Olympus TPLSM, with a total acquisition time of 30 min per video. During motility experiments, the blood vessels were labelled with 70-kDa dextran Texas Red (Invitrogen) which was intravenously injected before the imaging session. For evaluation of the BBB permeability, 3-kDa dextran Texas Red (Molecular Probes) was intravenously injected during the imaging session ($T = 0$).

Analysis of time-lapse videos and statistics. Acquired 3D time-lapse videos were analysed using Imaris 9.3.1 software (Bitplane AG). Cells were tracked using the automated Imaris Track module with subsequent manual revision. Motility parameters; that is, track length, track duration, track speed, track displacement and track straightness (ratio between total T cell path length and the sum of the entire single displacements), were calculated as described^{12,57} within a 30-min recording interval. Rolling T cells were defined as cells appearing as single or several round-shaped dots with an instantaneous velocity greater than 50 μ m per min.

RNA isolation, cDNA synthesis and quantitative PCR

Gene expression on transcription level was determined using quantitative PCR. RNA was extracted from TRI Reagent (Merck) according to the manufacturer's instructions. Reverse transcription into cDNA was performed using the RevertAid First Strand cDNA synthesis kit (Thermo Fisher Scientific) according to the manufacturer's instructions. Quantitative PCR was performed on an Applied Biosystems StepOnePlus Real-Time PCR system (Thermo Fisher Scientific) using custom-designed target-specific TaqMan probes quenched with TAMRA and labelled with FAM (Sigma-Aldrich). β -actin served as a housekeeping gene. All measurements were performed in duplicate. The difference in the CT values between the individual measurements did not exceed 0.5 amplification cycles. The combinations of primers and probes used to detect β -actin, integrins, cytokines, chemokines, chemokine receptors, cyclins and egression factors have previously been described^{12,17,57}. To detect the expression of tight junction genes, adhesion molecules, type I IFN-regulated genes and M2 macrophage markers the following combinations of primers and FAM-5'-3'-TAMRA probes were designed and tested:

Vcam1: Forward: ACATGAGGGTGCTCC TGTGA; Reverse: GGTGG CATTTCCTCGA GAGGA; Probe: TGTGCCAGCGAGGGT CTACC AGCTCCT. *Icam*: Forward: GGAGACAGCAGACCACTGTGCTT; Reverse: CTCGCTCTGGGAACG AATACA; Probe: ACTGTGGCACCACGC. *Cldn5*:

Forward: CGGGCGTCCAGAGTTCAGT; Reverse: GTCGACTCTTCC GC ATAGTCA; Probe: CCAGTCAAGTACTCA GCACCAAGGCCA. *Ocln*: Forward: CCTAATGTGGAAGAG TGGGTAAAAA; Reverse: GTCG ACTCTTTCCGC ATAGTCA; Probe: CACACAAGACATGCCTCCACCCCC. *Mxl1*: Forward: TCAA TTCAG AGTTCTTCTCGAGGAT; Reverse: GGGAG GTGAGC TCCATGGT; Probe: CCACAGTCCCTGCTTGGCAA. *Mx2*: Forward: GAAATCTTCCA GCATCTGAATGC; Reverse: AAATACTGGATG ATC AATGGAATGTG; Probe: TACCGCCAGGAGGCTCACAACCTGC. *Rsad2*: Forward: TTCCACACGGCCAAGACA; Reverse: ATACCAGCCTG TTTGAGCAGAAG; Probe: CCTTCGTGCTGCCCTGGAGG; *Irf8*: TGGTG ACTGGGTATACTGCCTATG; Reverse: TGCCCCGTAGTAAAAGTTGA; Probe: CGCACACCATTCAGCCTTATCCAG; *Irf7*: Forward: ACTTAGCC CGGAGCT TGGAT; Reverse: GCACTGCTGAGGGTCACTTCT; Probe: TACAATGGCCCC AGCTCTGGAGAACAG. *Oas1a*: Forward: GCGTCT GACTTGCCCTTGAG; Reverse: CGAGATACTGTCCACCCAGTGA; Probe: CCTTTGCTGAGGAGCCACCTTC. *Rtl-Ba*: Forward: GGTGAGAACAG CAAGCCAGTC; Reverse: GGTGAGGTAAGCCATCTT GTGG; Probe: TGAG ACCAGCTTCTTTCCAACCCTGA. *B2M*: Forward: TCAGAAAACCTCCCC AAATTCAAG; Reverse: GACACGTA GCAGTTGAGGAAGTTG; Probe: ACTCTCGCCATCCACCGGAGAATG. *Il6st*: Forward: ATCAATTTTG ACCCCGT GGAT; Reverse: TGGATAATTCTTCTGAGTTGGTCACT; Probe: AAGTGAAA CCCAGCCCACCTCATAATTTGT. *Arg1*: Forward: GAAAGTTCCAGATGTACCAGGAT; Reverse: AGCCGATGTACACGATG TCCTT; Probe: CTGGGTGACCCCTGCATATCTGC; *Mrc1*: Forward: CTGCAAAAAATCAGACGAAATCC; Reverse: TGTAGTAACAGTGGCC GTGGAA; Probe: TACGGAACCCCCACAGCTGCCTG. *Mrc1*: Forward: CTGCAAAAAATCAGA CGAAATCC; Reverse: TGTAGTAACAGTGGCC GTGGAA; Probe: TACGGAACCCCC ACAGCTGCCTG. *Ifnb1*: Forward: GCGTTCTGCTGTGCTTCTC; Reverse: TGCTAGTCTTGTGGAACTG; Probe: CACTGCCCTCTCCATCGACTACAAGCAG.

RNA extraction, cDNA library preparation and RNA sequencing

RNA extraction, cDNA library preparation, and RNA sequencing (RNA-seq) were performed as described^{11,57,58} at the Transcriptome and Genome Analysis Laboratory (TAL) of the University Medical Center Göttingen. For T cell sequencing, total RNA was isolated from T_{MBP} cells retrieved from the lungs of neomycin- or PBS-treated rats on day 0 and day 1 after intratracheal immunization. Three different biological replicates were prepared for each sample. For each replicate, around 20,000 T_{MBP} cells sorted from 4 to 5 rats with a purity greater than 98% were pooled. To address changes in the CNS expression profile after antibiotic treatments, total RNA from total spinal cord tissue or from spinal-cord-derived CD45^{low}CD11b⁺ microglial cells was isolated from rats that were intratracheally treated for 7 days with neomycin (1 mg per day), vancomycin (1 mg per day) or PBS. Three and five different biological replicates were prepared for total spinal cord and microglia samples, respectively. For each replicate, spinal cord samples of four to five rats were pooled. Between 20,000 and 40,000 cells were sorted from each pooled microglial sample with a purity greater than 98%. Library preparation for RNA-seq was performed using the TruSeq RNA Sample Preparation Kit (Illumina) starting from 300 ng of total RNA. Single read (45-bp) sequencing was conducted using a HiSeq 2000 (Illumina). Illumina BaseCaller software was used to transform fluorescence images into BCL files. Samples were demultiplexed to FASTQ files with CASAVA. FastQC software was used to check the sequencing quality. Sequences were aligned to the Ensembl reference genome of *Rattus norvegicus* allowing for 2 mismatches within 45 bases. Quantification of gene expression was done with the feature Counts program (v.1.5.1). Samples were subjected to differential expression analysis with DESeq2⁵⁹ (v.1.14.1). Gene annotation was performed using *Rattus norvegicus* entries from Ensembl. For analysis of T_{MBP} cells in the lung, genes with a minimum of one fold change and false discovery rate (FDR)-adjusted $P < 0.05$ were considered differentially expressed. For the analysis of sorted microglia and spinal cord, in which low differences in expression level were expected, genes with a minimum

of 0.5-fold change and FDR-adjusted $P < 0.05$ were considered differentially expressed. KEGG pathway and GO term enrichment analysis were performed using the Database for Annotation, Visualization and Integrated Discovery (DAVID)⁶⁰.

In vitro activation of microglia

Microglial cells were isolated from the spinal cords of PBS- or neomycin-treated rats using a three-phase Percoll density gradient as described^{11,61}. In brief, the spinal cord parenchyma was passed through a cell strainer (40 μ m) and washed once with PBS. Microglia were isolated from the 75%/50% isotonic Percoll interphase and washed once with PBS. Microglia from at least six rats per group were pooled. A total of 10,000 microglia per well were plated in flat bottom 96-well plates in 50 μ l DMEM-based medium containing 1% rat serum. Another 50 μ l of the above medium containing different concentrations of recombinant rat IFN γ were added to each well, resulting in final concentrations of 0, 1, 10 and 100 ng ml⁻¹ IFN γ . Before transfer, the microglia of each well were centrifuged at 1,500g for 4 min at 4 °C and the pellet was resuspended in 300 μ l TRI reagent (Merck) and 1 μ l glycogen (Roche). The samples were stored at -80 °C until further processing.

In vivo activation of microglia by intrathecal delivery of cytokines

For T-cell-independent activation of the microglia, rats were intravenously treated with PBS or neomycin. Seven days later, a cytokine mix (volume: 30 μ l) composed of IFN γ (250 ng) and TNF (250 ng) was injected in the cisterna magna of anaesthetized rats. Rats were analysed 4 and 18 h after intrathecal injection. The cytokines IFN γ and TNF were selected because of their essential role in triggering CNS autoimmunity in rats^{11,62}. The final cytokine dose and the analysis time points were chosen on the basis of preliminary experiments (data not shown) in which the cytokines were titrated and their effect on the CNS was measured at different time intervals after injection.

Histology and immunohistochemistry

Rats underwent treatment with PBS or neomycin for 7 days before intracardial perfusion with cold saline solution (10 min) followed by a cold fixative containing 4% PFA (15 min). Samples were post-fixed in the same fixative for 24 h and then equilibrated in a 30% sucrose solution. Thereafter, brains and spinal cords were embedded in cryoprotectant and stored at -20 °C. Brains and spinal cords were cut into 50- μ m-thick coronal sections (brain coordinates from bregma: -1.92 to -3.72, spinal cord: L1 to L6) using a cryostat (Leica) and stored in PBS at 4 °C until further use.

The sections were permeabilized and washed in PBS containing 0.3% Triton X-100. The blocking was performed with serum (5%) from the secondary antibody host(s) for 1.5 h at room temperature. Thereafter, the slices were incubated with the primary antibodies in blocking solution (5%) for 48 h at 4 °C. This step was followed by an overnight incubation at 4 °C with the suitable fluorophore-conjugated secondary antibodies in blocking solution (3%). The sections were then mounted on SuperFrostPlus Slides (Thermo Fisher Scientific) with Fluoromount-G (Southern Biotech). For microglia analysis (brain and spinal cord), anti-IBA-1 (1:500; rabbit; polyclonal; Wako 019-19741) and Rhodamine Red-X (RRX) anti-rabbit (1:200; donkey; polyclonal; Jackson 711-295-152) were used as first and secondary antibody, respectively.

Images were acquired with a Zeiss Laser Scanning Microscope 710 (Carl Zeiss) controlled by Zeiss ZEN 2012 SP2 v.2.1 software (Carl Zeiss) equipped with UV-diode for DAPI, a 488 nm Argon laser, a 561 nm DPSS laser and a 633 nm HeNe laser. Lasers were routed through a 40 \times oil NAL3 immersion objective Plan Apochromat objective (Carl Zeiss). The pinhole size was set to 50 μ m. A z-step size between 0.5 and 1 μ m was chosen for optimal z-resolution. Morphological analysis and three-dimensional reconstruction of microglia was performed using Imaris 8.0.1 software (Bitplane AG) as described¹¹. Confocal z-stacks were smoothed with both

Article

Median and Gaussian filters. Single cells were rendered by first using the filament tool to reconstruct the processes and later the surface tool to render the cell body. The 3D-rendered images served for the quantitative analysis of morphological parameters.

Statistical analysis

Statistical analysis was performed using GraphPad Prism (v.6–8; GraphPad) and Microsoft Excel (2010 and 2016; Microsoft). Unless indicated otherwise, data are represented as mean \pm s.e.m. (standard error of the mean). The statistical significance is reported in the figures. The statistical tests that underlie the data analysis are stated in the corresponding figure legends. In brief, Gaussian distribution of independent datasets was tested using a Kolmogorov–Smirnov test with Lilliefors' correction. For comparing two datasets, statistical significance was determined by unpaired two-tailed *t*-test in the case of Gaussian and Mann–Whitney test in the case of non-Gaussian distribution. For comparing more than two datasets, statistical significance was determined by one-way ANOVA with Tukey's multiple comparisons test in the case of Gaussian and Kruskal–Wallis test with Dunn's multiple comparisons test in the case of non-Gaussian distribution. In the case of the number of animals per experiment not being sufficient to test for normality, Gaussian distribution was assumed unless differently indicated. Significance levels were set as $*P < 0.05$, $**P < 0.01$, $***P < 0.001$.

Reporting summary

Further information on research design is available in the Nature Research Reporting Summary linked to this paper.

Data availability

RNA-seq datasets have been deposited online in the Gene Expression Omnibus (GEO) and BioProject with accession codes GSE191287, GSE192411 and PRJNA789820. Source data are provided with this paper.

46. Määttä, J. A., Coffey, E. T., Hermonen, J. A., Salmi, A. A. & Hinkkanen, A. E. Detection of myelin basic protein isoforms by organic concentration. *Biochem. Biophys. Res. Commun.* **238**, 498–502 (1997).
47. Murray, C. et al. Interdependent and independent roles of type I interferons and IL-6 in innate immune, neuroinflammatory and sickness behaviour responses to systemic poly I:C. *Brain Behav. Immun.* **48**, 274–286 (2015).
48. Rittirsch, D. et al. Acute lung injury induced by lipopolysaccharide is independent of complement activation. *J. Immunol.* **180**, 7664–7672 (2008).
49. Klindworth, A. et al. Evaluation of general 16S ribosomal RNA gene PCR primers for classical and next-generation sequencing-based diversity studies. *Nucleic Acids Res.* **41**, e1 (2013).
50. von Hoyningen-Huene, A. J. E. et al. Bacterial succession along a sediment porewater gradient at Lake Neusiedl in Austria. *Sci. Data* **6**, 163 (2019).

51. Rognes, T., Flouri, T., Nichols, B., Quince, C. & Mahé, F. VSEARCH: a versatile open source tool for metagenomics. *PeerJ* **4**, e2584 (2016).
52. Yilmaz, P. et al. The SILVA and "All-species Living Tree Project (LTP)" taxonomic frameworks. *Nucleic Acids Res.* **42**, D643–D648 (2014).
53. Quast, C. et al. The SILVA ribosomal RNA gene database project: improved data processing and web-based tools. *Nucleic Acids Res.* **41**, D590–D596 (2013).
54. Chen, L. et al. GMPR: a robust normalization method for zero-inflated count data with application to microbiome sequencing data. *PeerJ* **6**, e4600 (2018).
55. Andersen, K. S., Kirkegaard, R. H., Karst, S. M. & Albertsen, M. ampvis2: an R package to analyse and visualise 16S rRNA amplicon data. Preprint at <https://doi.org/10.1101/299537> (2018).
56. Wickham, H. ggplot2: Elegant Graphics for Data Analysis (Springer, 2016).
57. Schläger, C. et al. Effector T-cell trafficking between the leptomeninges and the cerebrospinal fluid. *Nature* **530**, 349–353 (2016).
58. Cabeza, R. et al. An RNA sequencing transcriptome analysis reveals novel insights into molecular aspects of the nitrate impact on the nodule activity of *Medicago truncatula*. *Plant Physiol.* **164**, 400–411 (2014).
59. Love, M. I., Huber, W. & Anders, S. Moderated estimation of fold change and dispersion for RNA-seq data with DESeq2. *Genome Biol.* **15**, 550 (2014).
60. Huang, D. W., Sherman, B. T. & Lempicki, R. A. Systematic and integrative analysis of large gene lists using DAVID bioinformatics resources. *Nat. Protoc.* **4**, 44–57 (2009).
61. Doorn, K. J. et al. Brain region-specific gene expression profiles in freshly isolated rat microglia. *Front. Cell. Neurosci.* **9**, 84 (2015).
62. Klinkert, W. E. et al. TNF- α receptor fusion protein prevents experimental auto-immune encephalomyelitis and demyelination in Lewis rats: an overview. *J. Neuroimmunol.* **72**, 163–168 (1997).

Acknowledgements We thank S. Schwarz for helping in the quantification of the *tuf* gene expression; M. Ulisse for contributing to characterizing the lung immune milieu; G. Salinas for performing the transcriptome analyses; O. Shomroni for the analysis of the transcriptome data; S. Hamann, M. Weig and M. Heinemann for technical assistance; A. Poehlein for performing the 16S rRNA sequencing; D. Schneider for providing the bioinformatic amplicon processing pipeline; D. Miljković for helping with animal experiments and reading the manuscript; and C. Ludwig for text editing. This work was supported by the Deutsche Forschungsgemeinschaft (DFG, German Research Foundation) RK-Grant FL 377/3-1; FL 377/2-2; SFB 1328/1 project A01, project no. 335447717; OD 87/1-1, OD 87/3-1; SFB TRR 274/1 2020 projects A03 and A04, project no. 408885537; and by the European Commission under the European Union's Horizon 2020 research and innovation programme, grant agreement no. 101021345 (T-Neuron). L.H. is supported by the Klaus Faber Stiftung.

Author contributions L.H. performed most experimental work and together with A.F. and F.O. wrote the paper. R.C.C. contributed to immune cell characterizations by quantitative PCR analyses and flow cytometry and by performing EAE experiments. F.J.v.d.F. performed the intravital TPLSM and supported L.H. with inducing and analysing autoimmune models. J.H. contributed with the microbiome analyses, and R.D. contributed with his expertise in microbiome biology and interpretation of the microbiota sequencing data. A.F. together with F.O. designed the study, coordinated the experimental work and wrote the manuscript with inputs from co-authors.

Competing interests The authors declare no competing interests.

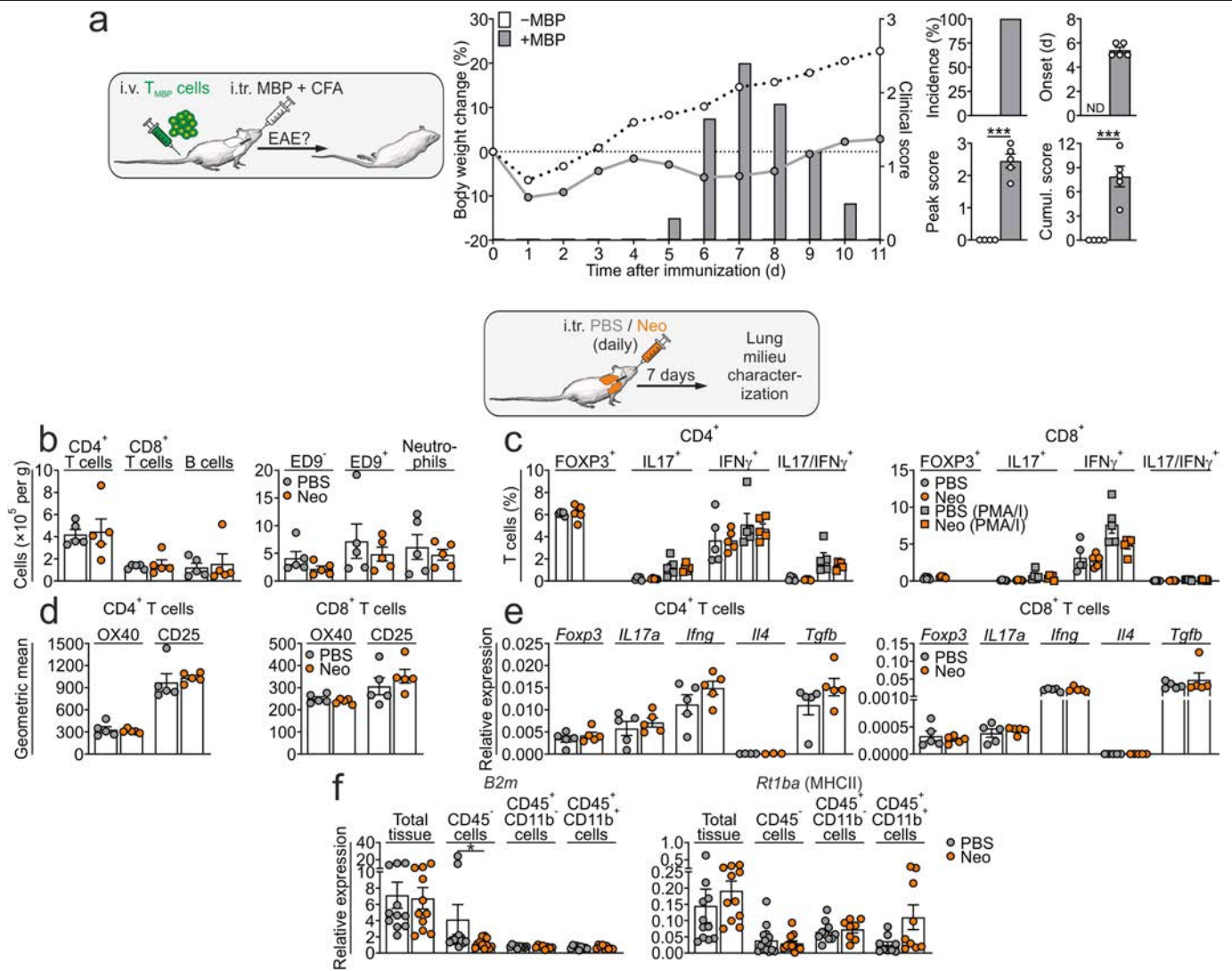
Additional information

Supplementary information The online version contains supplementary material available at <https://doi.org/10.1038/s41586-022-04427-4>.

Correspondence and requests for materials should be addressed to Francesca Odoardi.

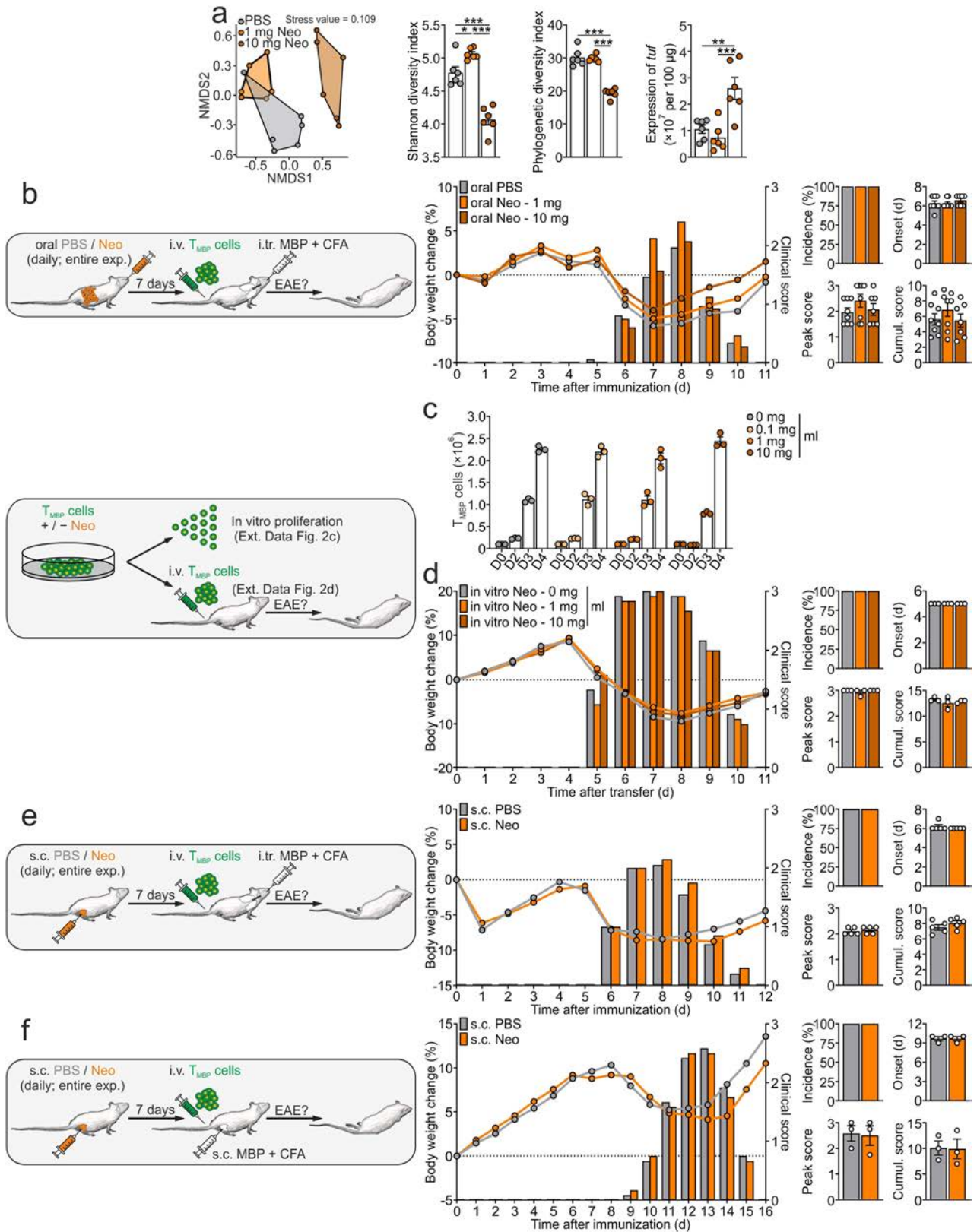
Peer review information *Nature* thanks Sarkis Mazmanian, Vijay Kuchroo and the other, anonymous, reviewer(s) for their contribution to the peer review of this work.

Reprints and permissions information is available at <http://www.nature.com/reprints>.



Extended Data Fig. 1 | Establishment of a lung EAE model and targeted manipulation of the lung microbiome. **a**, Lung EAE. Rats were intravenously (i.v.) transferred with resting T_{MBP} cells and 6 h later were intratracheally (i.tr.) immunized with CFA \pm MBP. Clinical parameters: Body weight change (lines) and clinical scores (bars) over the EAE course, incidence (%), onset (days after immunization), peak score, cumulative score. Mean \pm s.e.m. Representative data of 3 independent experiments. $n = 4$ (-MBP); $n = 5$ (+MBP). ND, not determinable. **b–e**, I.tr. neomycin (Neo) treatment does not change the lung immune cell composition. Lung samples were isolated from rats i.tr. treated for 7 days with PBS or neomycin. **b**, Number of endogenous $\alpha\beta$ TCR⁺ CD4⁺ and CD8⁺ T cells, CD45RA⁺ B cells, CD11b⁺ ED9⁻ interstitial macrophages, CD11b⁺ ED9⁺ M Φ (alveolar macrophages and infiltrating monocytes) and RP3⁺ neutrophils. Flow cytometry. Mean \pm s.e.m. **c**, Percentage expression of FoxP3, IFN γ and IL17 in endogenous $\alpha\beta$ TCR⁺ CD4⁺ and CD8⁺ T cells. Flow cytometry. IFN γ and IL17 were

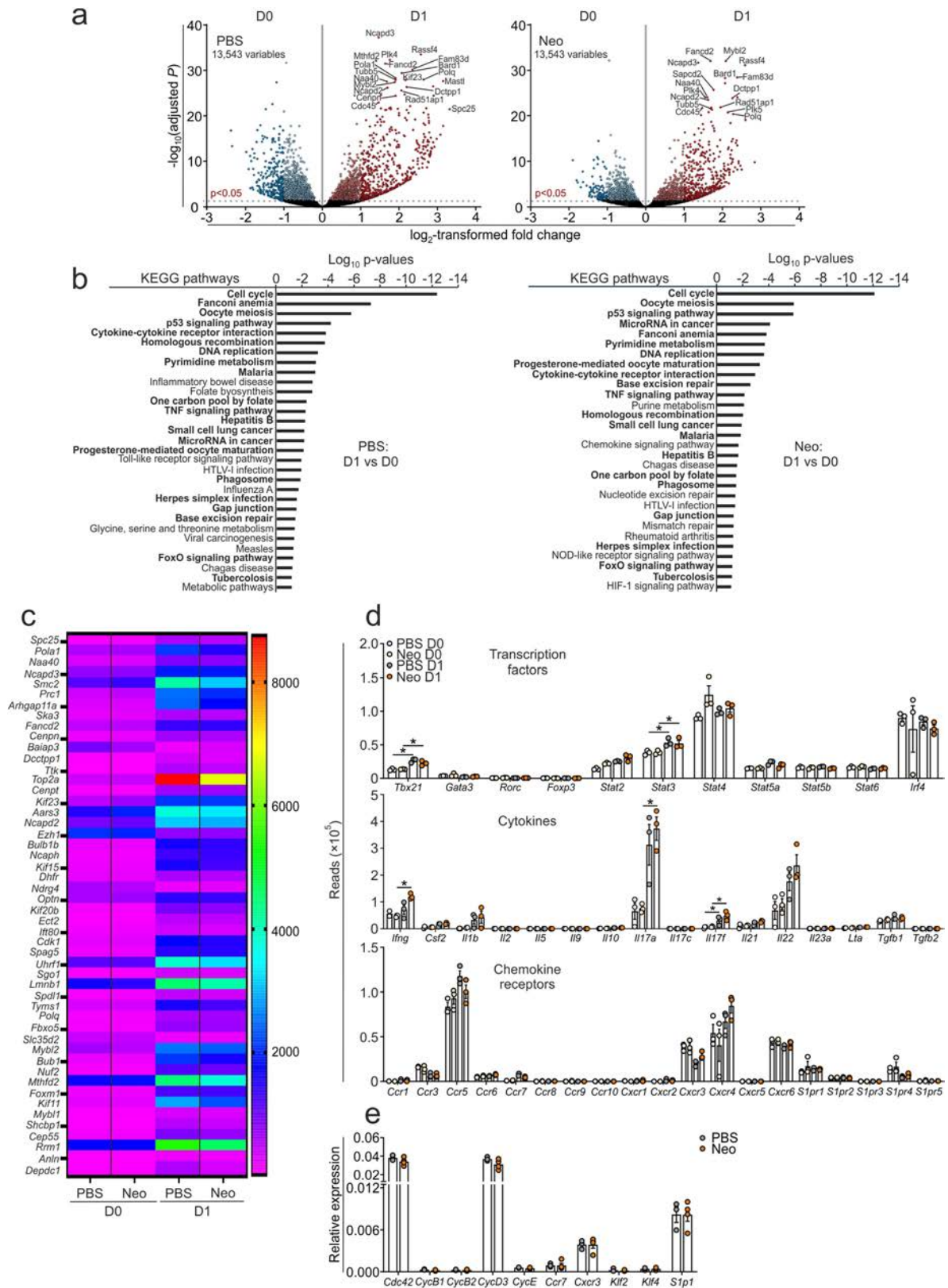
analysed in steady state condition and upon stimulation with PMA and Ionomycin (PMA/I). Mean \pm s.e.m. **d, e**, Corresponding surface expression of the activation markers CD134 (OX40) and CD25 (IL2R) by flow cytometry (d) and expression of the indicated cytokines measured by quantitative PCR (e) Mean \pm s.e.m. **b–e**, Cumulative data of 2 independent experiments. $n = 5$ (all groups). **f**, I.tr. treatment for 7 days with PBS or neomycin does not change MHC expression in lung immune cells. Expression of the indicated genes in total lung, pulmonary stromal cells (CD45⁺), as well as lymphoid (CD45⁺ CD11b⁺) or myeloid (CD45⁻ CD11b⁺) hematopoietic pulmonary cell populations. Quantitative PCR. Housekeeping gene: β -actin. Mean \pm s.e.m. Cumulative data of 3 independent experiments. $n = 9–14$ (PBS); $n = 8–12$ (Neo) per condition. **a–f**, Statistical significance determined by unpaired two-tailed *t*-test (Gaussian distribution) and Mann–Whitney test (non-Gaussian distribution). * $P < 0.05$, ** $P < 0.01$, *** $P < 0.001$.



Extended Data Fig. 2 | See next page for caption.

Extended Data Fig. 2 | Neomycin treatment outside the lung does not affect CNS autoimmunity. **a, b**, Oral treatment with neomycin does not ameliorate EAE. **a**, Left, PCA of the microbiota composition of faecal samples from rats that were orally treated with neomycin (1 or 10 mg) or PBS for 7 days. Middle, corresponding Shannon and phylogenetic diversity indices. Right, quantification of bacterial abundance based on *tuf* gene expression via 16S rRNA-based quantitative PCR. Mean \pm s.e.m. Cumulative data of 2 independent experiments. $n = 6$ (all groups). **b**, Clinical parameters observed in lung EAE of rats pre-treated orally with PBS or neomycin (1 or 10 mg) for 7 days. Mean \pm s.e.m. Cumulative data of 2 independent experiments. $n = 8$ (PBS, 1 mg Neo); $n = 7$ (10 mg Neo). **c, d**, I.t.r. neomycin treatment does not affect T_{MBP} cell proliferation and effector function. **c**, Quantification of T_{MBP} cells cultured in presence of neomycin at the indicated concentrations. Flow cytometry on D2, D3 and D4 after antigen challenge. Representative data of 2 independent experiments. $n = 3$ (all groups). **d**, Clinical outcome of EAE induced by transfer

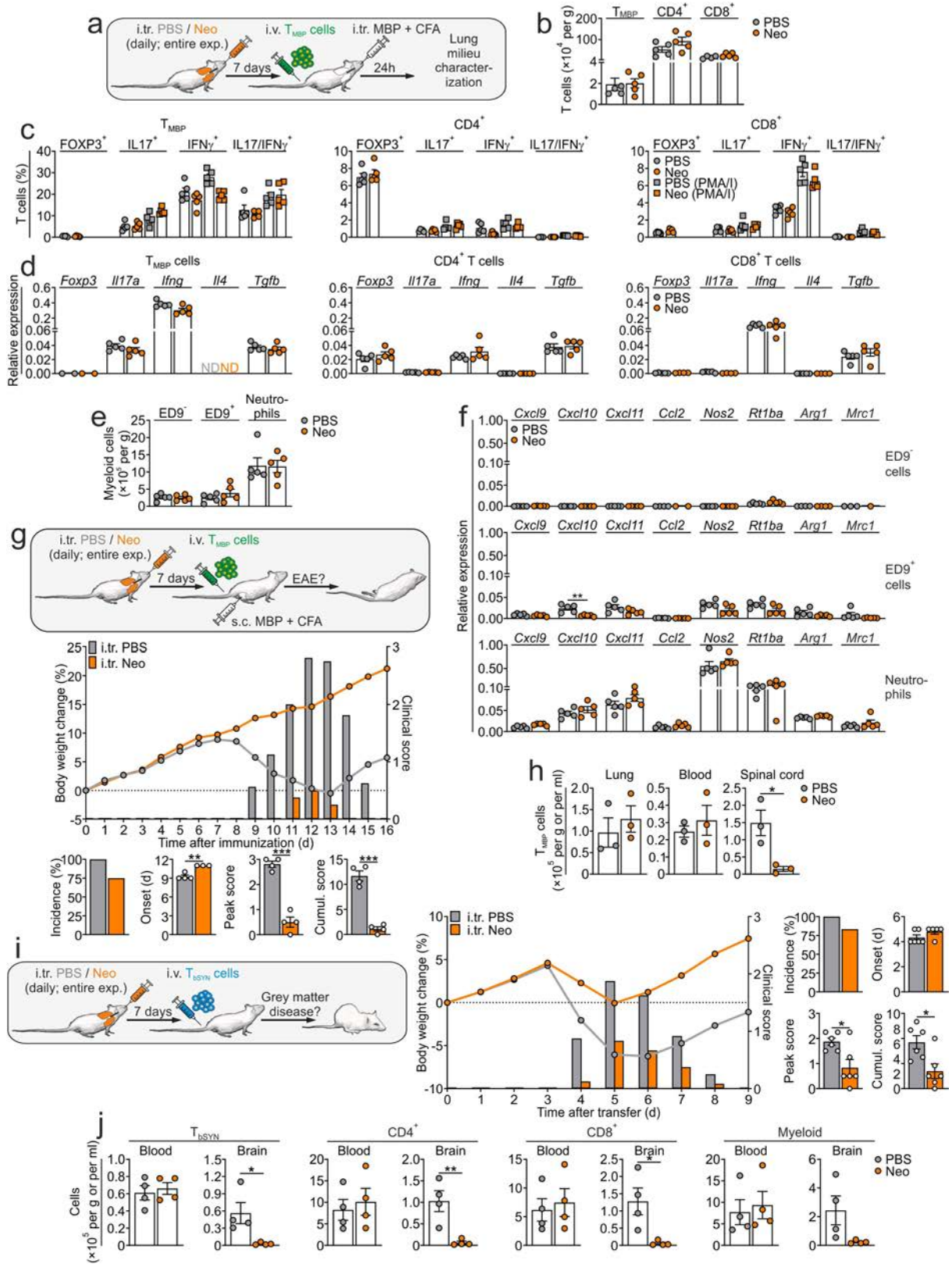
of T_{MBP} cells previously stimulated in vitro in presence of neomycin at the indicated concentrations. Clinical parameters. Mean \pm s.e.m. Representative data of 3 independent experiments. $n = 3$ (both groups). **e, f**, Subcutaneous (s.c.) treatment with neomycin does not affect EAE. **e**, Lung EAE was induced in rats s.c. pre-treated for 7 days with PBS or neomycin. Clinical parameters. Mean \pm s.e.m. Representative data of 3 independent experiments. $n = 5$ (both groups). **f**, Rats s.c. pre-treated for 7 days with PBS or neomycin were i.v. transferred with resting T_{MBP} cells. 6 h later, they were s.c. immunized with MBP. Clinical parameters. Mean \pm s.e.m. Representative data of 3 independent experiments. $n = 3$ (both groups). **a-d**, Statistical significance determined by one-way ANOVA with Tukey's multiple comparisons test (Gaussian distribution) and Kruskal-Wallis test with Dunn's multiple comparisons test (non-Gaussian distribution). **e, f**, Statistical significance determined by unpaired two-tailed *t*-test (Gaussian distribution) and Mann-Whitney test (non-Gaussian distribution). * $P < 0.05$, ** $P < 0.01$, *** $P < 0.001$.



Extended Data Fig. 3 | See next page for caption.

Extended Data Fig. 3 | Lung dysbiosis does not modify T cell activation and expression profile in the lung. a–e, Lung EAE was induced in rats that were pre-treated i.tr. with neomycin or PBS for 7 days. **a**, Lung immunization induces reprogramming in the gene expression profile of T_{MBP} cells. Volcano plots depicting the differential gene expression profiles of lung-derived T_{MBP} cells from PBS- (left) or neomycin- (right) pre-treated rats between D1 and D0 after immunization. Red and blue dots represent significantly up- or downregulated genes ($P < 0.05$), respectively. Indicated are representative genes involved in cell division and cell cycle. **b, c**, Genes differentially expressed after immunization are mainly involved in cell cycle. **b**, Significantly regulated KEGG pathways for genes upregulated between D1 versus D0 after immunization in T_{MBP} cells isolated from lung of PBS- (left) or neomycin-treated (right) rats.

b, c, Heat map of the 50 most upregulated genes in D1 versus D0 after immunization in PBS- and neomycin-treated rats. **d**, Lung immunization does not change effector T cell differentiation. Total reads of transcription factors, cytokines and chemokine receptors in T_{MBP} cells isolated from lung of PBS- or neomycin-treated rats on D0 and D1 after immunization Mean \pm s.e.m. $n = 3$ (all groups). **e**, I.tr. neomycin treatment does not impair T_{MBP} cell activation and migratory program. Relative expression of chemokine receptors and genes involved in cell cycle and cell egress in T_{MBP} cells isolated from the lung of PBS- or neomycin-pre-treated rats on D1 after immunization. Quantitative PCR. Mean \pm s.e.m. Representative data of two independent experiments. $n = 3$ (PBS); $n = 4$ (Neo) per condition. **d, e**, Statistical significance determined by unpaired two-tailed t -test. $*P < 0.05$.

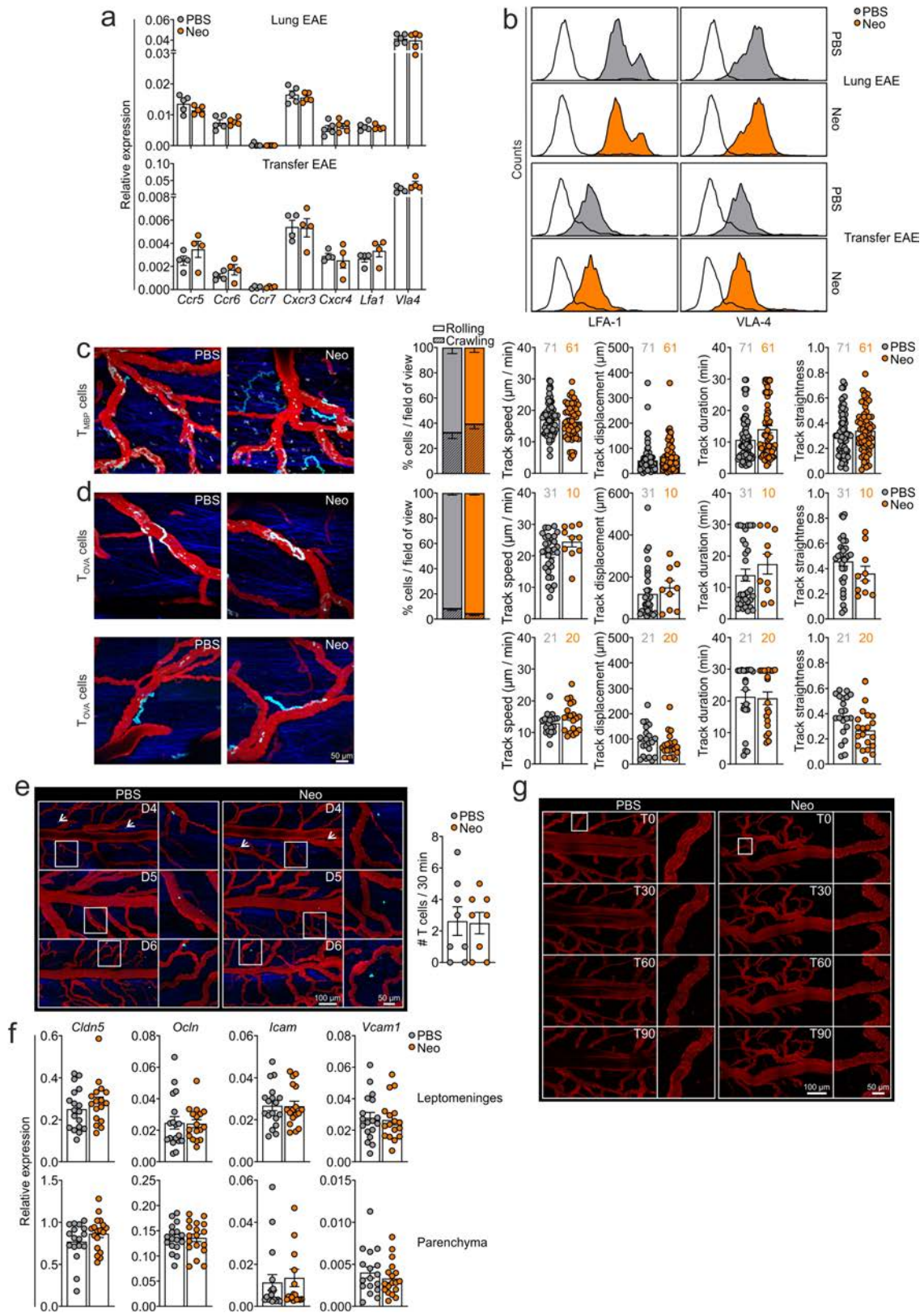


Extended Data Fig. 4 | See next page for caption.

Extended Data Fig. 4 | Lung dysbiosis does not impair the lung immune response after immunization but impairs grey matter autoimmunity.

a–f, Lung EAE was induced in rats pre-treated i.tr. with PBS or neomycin. Characterization of the lung immune milieu was performed 24 h after i.tr. immunization. **a**, Lung EAE was induced in rats that were pre-treated i.tr. with neomycin or PBS for 7 days. **b–d**, Lung microbiome dysbiosis does not impair local T cell responses. **b**, Absolute numbers of T_{MBP} cells and endogenous $\alpha\beta TCR^+ CD4^+$ and $CD8^+$ T cells. Flow cytometry. **c**, Corresponding percentage expression of FoxP3 and proinflammatory cytokines in stimulated (PMA/I) or non-stimulated T cell subsets. Flow cytometry. Representative data from 2 independent experiments. $n = 5$ (all groups). **d**, Relative expression of the indicated T cell lineage-signature cytokines in each T cell subset. Quantitative PCR. Housekeeping gene: β -actin. Mean \pm s.e.m. **b–d**, Representative data from 2 independent experiments. $n = 5$ (all groups). **e, f**, Lung microbiome dysbiosis does not impair local myeloid cell responses. **e**, Absolute number of $CD11b^+ ED9^-$ interstitial macrophages, $CD11b^+ ED9^+$ M Φ and $RP3^+$ neutrophils. Flow cytometry. **f**, Corresponding expression of chemokines, iNOS (*Nos2*), MHC-II (*RtIba*) and M2 macrophage markers. Quantitative PCR. Housekeeping gene:

β -actin. **e–f**, Mean \pm s.e.m. Representative data of 2 independent experiments. $n = 5$ (all groups). **g, h**, Lung dysbiosis prevents T_{MBP} cell entry into the CNS and ameliorates peripheral EAE induced by s.c. immunization. Rats were i.tr. treated with neomycin or PBS for 7 days. Subsequently, they were i.v. transferred with resting T_{MBP} cells and s.c. immunized with MBP. **g**, Clinical parameters. Mean \pm s.e.m. Representative data of 3 independent experiments. $n = 4$ (both groups). **h**, Number of T_{MBP} cells detected in the indicated organs by flow cytometry on D11 after immunization. Mean \pm s.e.m. Representative data of 3 independent experiments. $n = 3$ (both groups). **i, j**, I.tr. neomycin treatment reduces T_{bSYN} cell entry in the brain and ameliorates autoimmune grey matter disease. Grey matter autoimmunity was induced in rats pre-treated with neomycin or PBS by transfer of T_{bSYN} cells. **i**, Clinical parameters. Mean \pm s.e.m. Cumulative data of 2 independent experiments. $n = 6$ (both groups). **j**, Quantification of the indicated immune cell subsets in blood or brain on D5 after transfer. Flow cytometry. Mean \pm s.e.m. Representative data of 2 independent experiments. $n = 4$ (both groups). **b–j**, Statistical significance determined by unpaired two-tailed *t*-test (Gaussian distribution) and Mann-Whitney test (non-Gaussian distribution). * $P < 0.05$, ** $P < 0.01$, *** $P < 0.001$.

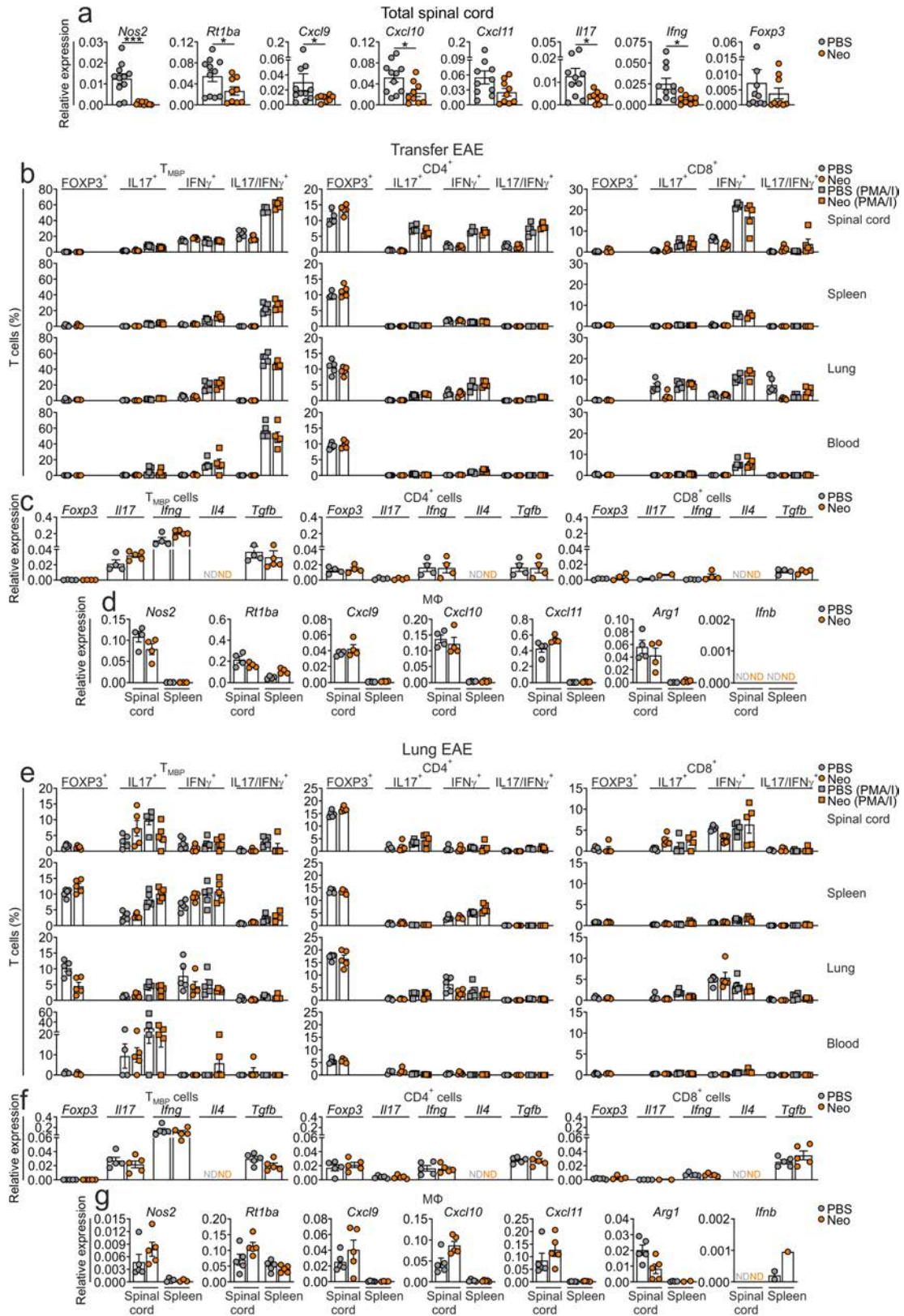


Extended Data Fig. 5 | See next page for caption.

Extended Data Fig. 5 | Lung dysbiosis affects neither T cell and endothelial cell interactions at the CNS borders nor the barrier integrity. a, b, I.tr.

neomycin treatment does not influence the expression of either chemokine receptors or adhesion molecules in T_{MBP} cells. Lung EAE or transfer EAE were induced in PBS- or neomycin- pre-treated rats. **a**, Chemokine receptor and integrin expression in T_{MBP} cells isolated from blood on D5 after immunization (lung EAE, $n = 5$ per condition) or D4 after transfer (transfer EAE, $n = 4$ per condition). Quantitative PCR. Housekeeping gene: β -actin. Mean \pm s.e.m. Representative data of 2 independent experiments. **b**, Corresponding protein expression of LFA-1 and VLA-4. Flow cytometry. Representative data of 2 independent experiments. **c, d**, I.tr. neomycin treatment does not affect T cell motility at the CNS borders. T_{MBP} (c) or T_{OVA} (d) cells were i.v. transferred into rats pre-treated with PBS or neomycin. **c**, Intravascular T_{MBP} cell motility was recorded in the leptomeninges by TPLSM on D2.5 post transfer. Depicted are representative time-projection images over a period of 30 min, percentage of crawling versus rolling cells ($n = 8$ videos per group) and quantification of the indicated motility parameters. Number of analysed T cells is indicated. Mean \pm s.e.m. Representative data of 2 independent experiments. $n = 2-4$ (both groups). Turquoise, T_{MBP} cells; Red, 70 kDa Texas Red Dextran labelled vessels; Blue, Collagen. **d**, Intravascular (upper panel) and extravascular (lower panel) T_{OVA} cell motility was recorded in the leptomeninges by TPLSM on D3 and D4 post transfer, respectively. Time projection images over a period of 30 min, percentage of crawling versus rolling cells ($n = 9$ videos per group) and intravascular and extravascular motility parameters derived from the indicated number of T cells. Mean \pm s.e.m. Turquoise, T_{OVA} cells; Red, 70 kDa

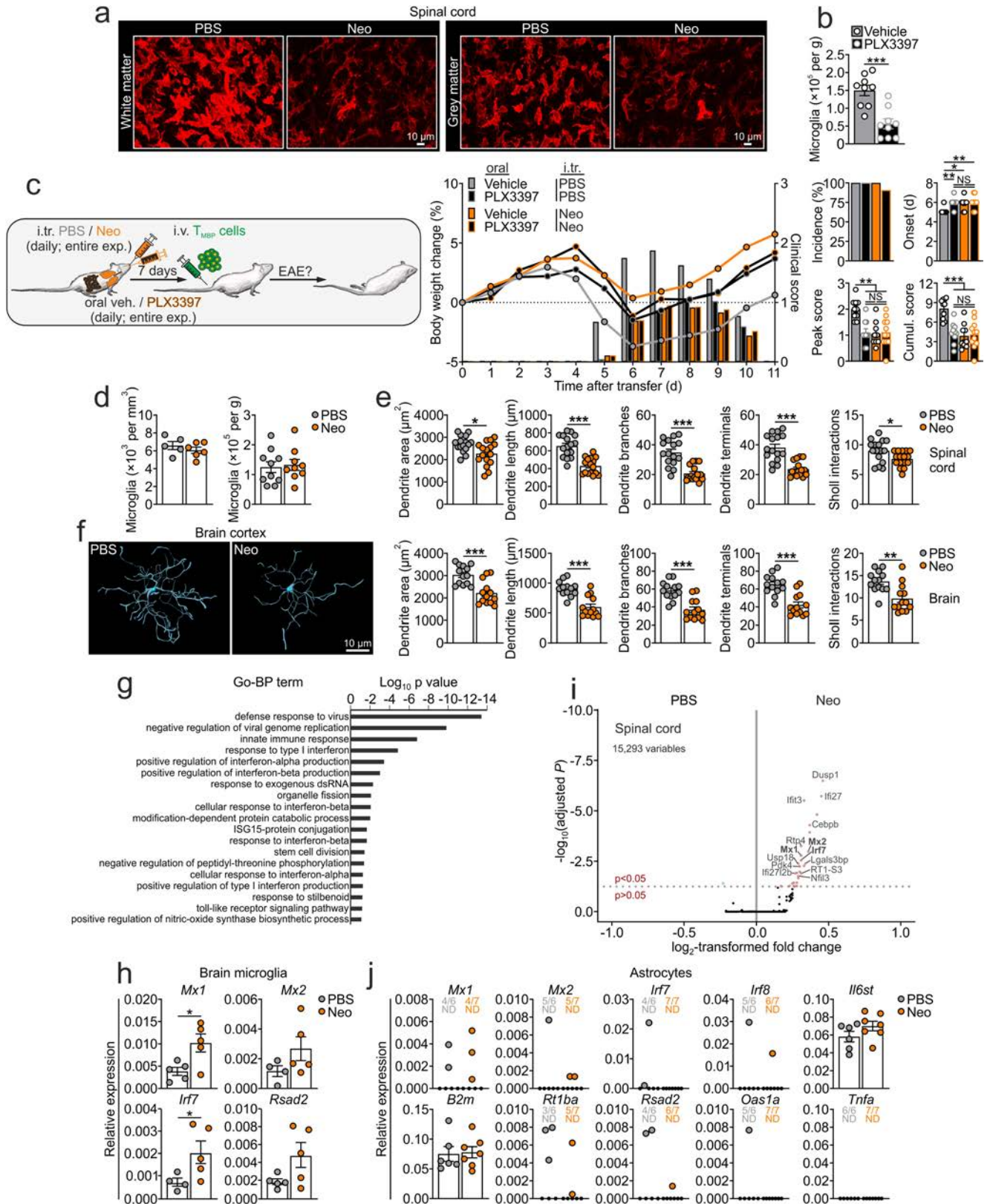
Texas Red Dextran labelled vessels; Blue, Collagen. **e**, I.tr. neomycin treatment does not affect T_{OVA} cell diapedesis. Intravital TPLSM overviews and corresponding magnified pictures depicting the distribution of T_{OVA} cells (turquoise) in the leptomeningeal milieu at the indicated time points post transfer in PBS- or neomycin- pre-treated rats. Red, 70 kDa dextran Texas-Red labelled vessels; Blue, Collagen. Arrows, Representative T_{OVA} cells. Graph, Corresponding quantification of T_{OVA} cells in the extravascular environment. Each dot represents a single 30 min video. Mean \pm SEM. Representative data of two independent experiments. $n = 8$ (both groups). **f**, I.tr. neomycin treatment does not change the expression of tight junction molecules and integrin ligands. Expression of the indicated genes in endothelial cells isolated from spinal cord leptomeninges and parenchyma of rats pre-treated for 7 days with PBS or neomycin. Quantitative PCR. Housekeeping gene: β -actin. Mean \pm s.e.m. Cumulative data of 4 independent experiments. $n = 17-18$ (all groups). **g**, I.tr. neomycin treatment does not alter the permeability of leptomeningeal vessels. Intravital TPLSM overviews and corresponding magnified pictures of the thoracic spinal cord recorded 7 days after i.tr. PBS or neomycin treatment. Images were acquired 0, 30, 60 and 90 min after i.v. injection of 3 kDa Texas Red Dextran. No leakage of the dye was observed at any time point. Representative images from two independent experiments. **a, e, f**, Statistical significance determined by unpaired two-tailed t -test (Gaussian distribution) and Mann-Whitney test (non-Gaussian distribution). **c, d**, Statistical significance of percentage crawling versus rolling was determined with a two-way ANOVA; for the other motility parameters unpaired two-tailed t -test (Gaussian distribution) and Mann-Whitney test (non-Gaussian distribution) were used.



Extended Data Fig. 6 | See next page for caption.

Extended Data Fig. 6 | Lung dysbiosis induces quantitative but not qualitative changes in the immune infiltrates in the CNS. **a**, I.tr. neomycin treatment reduces T_{MBP} cell-mediated CNS inflammation. Expression of iNOS (*Nos2*), MHC-II (*Rt1ba*), chemokines, proinflammatory cytokines and regulatory genes in total spinal cord at the initiation stage of the EAE (i.e. 24 h after the onset of the clinical symptoms). Quantitative PCR. Housekeeping gene: β -actin. Mean \pm s.e.m. $n = 11$ (PBS); $n = 9$ (Neo). **b**, **c**, T cell responses in the CNS are not affected by lung dysbiosis in transfer EAE. EAE was induced in rats pre-treated i.tr. with neomycin or PBS by transfer of T_{MBP} cells. Immune cell characterization was performed at the initiation stage of the disease. **b**, Percentage of T_{MBP} cells, endogenous $\alpha\beta$ TCR⁺ CD4⁺ and CD8⁺ T cells expressing FoxP3 and proinflammatory cytokines (steady state and PMA/I-stimulated conditions) in the CNS and in the indicated peripheral compartments. Flow cytometry. Mean \pm s.e.m. Representative data of 2 independent experiments. $n = 5$ (all groups). **c**, Corresponding expression of the specified T cell lineage signature cytokines in the indicated T cell subsets isolated from the spinal cord. Quantitative PCR. Housekeeping gene: β -actin. Mean \pm s.e.m. $n = 2-4$ (all groups). **d**, Myeloid cells recruited to the CNS are not impaired by lung dysbiosis. Expression of iNOS (*Nos2*), MHC-II (*Rt1ba*), chemokines, M2 macrophage marker and IFN β in spleen-derived CD45^{high}

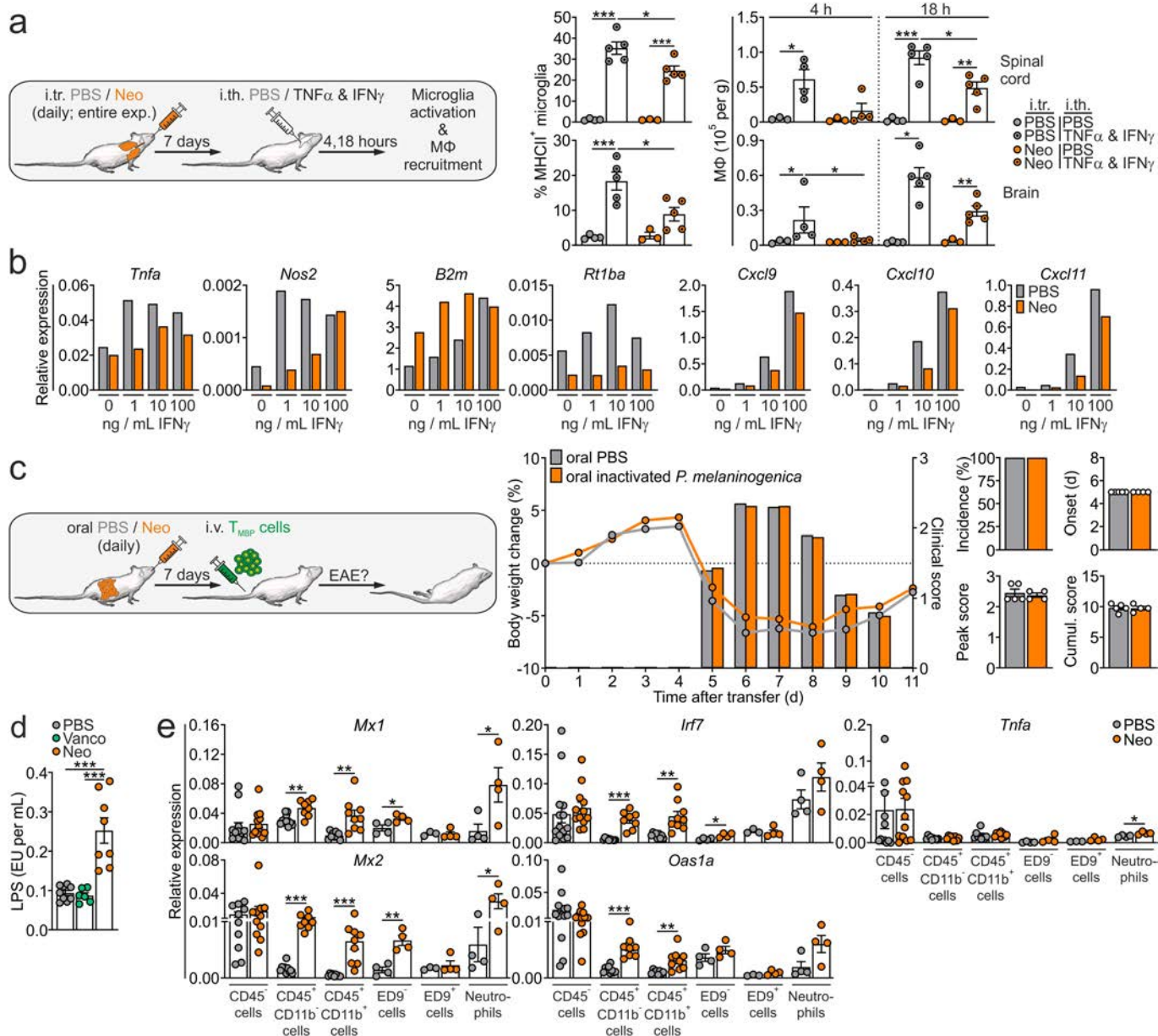
CD11b⁺ M Φ and in CNS-derived CD45^{high} CD11b⁺ M Φ at the initiation stage of EAE. Quantitative PCR. Housekeeping gene: β -actin. Mean \pm s.e.m. Representative data of 2 independent experiments. $n = 3-4$ (PBS); $n = 4$ (Neo) per condition. **e**, T cell response in the CNS is not affected by lung dysbiosis also in lung active EAE. Lung EAE was induced in rats pre-treated i.tr. with neomycin or PBS. Immune cell analysis was performed at the initiation stage of the disease. **e**, Percentage of T_{MBP} cells, endogenous $\alpha\beta$ TCR⁺ CD4⁺ and CD8⁺ T cells expressing FoxP3 and proinflammatory cytokines (steady state and PMA/I-stimulated conditions) in the CNS and in the indicated peripheral compartments. Flow cytometry. Mean \pm s.e.m. Representative data of 2 independent experiments. $n = 5$ (all groups). **f**, Corresponding expression of the specified T cell lineage-signature cytokines measured as in **c**. Quantitative PCR. Mean \pm s.e.m. $n = 2-5$ (all groups). **g**, Myeloid cells recruited to the CNS are not functionally impaired. Expression of the indicated genes measured as in **d** in spleen-derived CD45^{high} CD11b⁺ M Φ and in CNS-derived CD45^{high} CD11b⁺ M Φ . Quantitative PCR. Mean \pm s.e.m. Representative data of 2 independent experiments. $n = 2-5$ (all groups). **a-g**, Statistical significance was determined by unpaired two-tailed *t*-test (Gaussian distribution) and Mann-Whitney test (non-Gaussian distribution). * $P < 0.05$, *** $P < 0.001$; ND, not detected.



Extended Data Fig. 7 | See next page for caption.

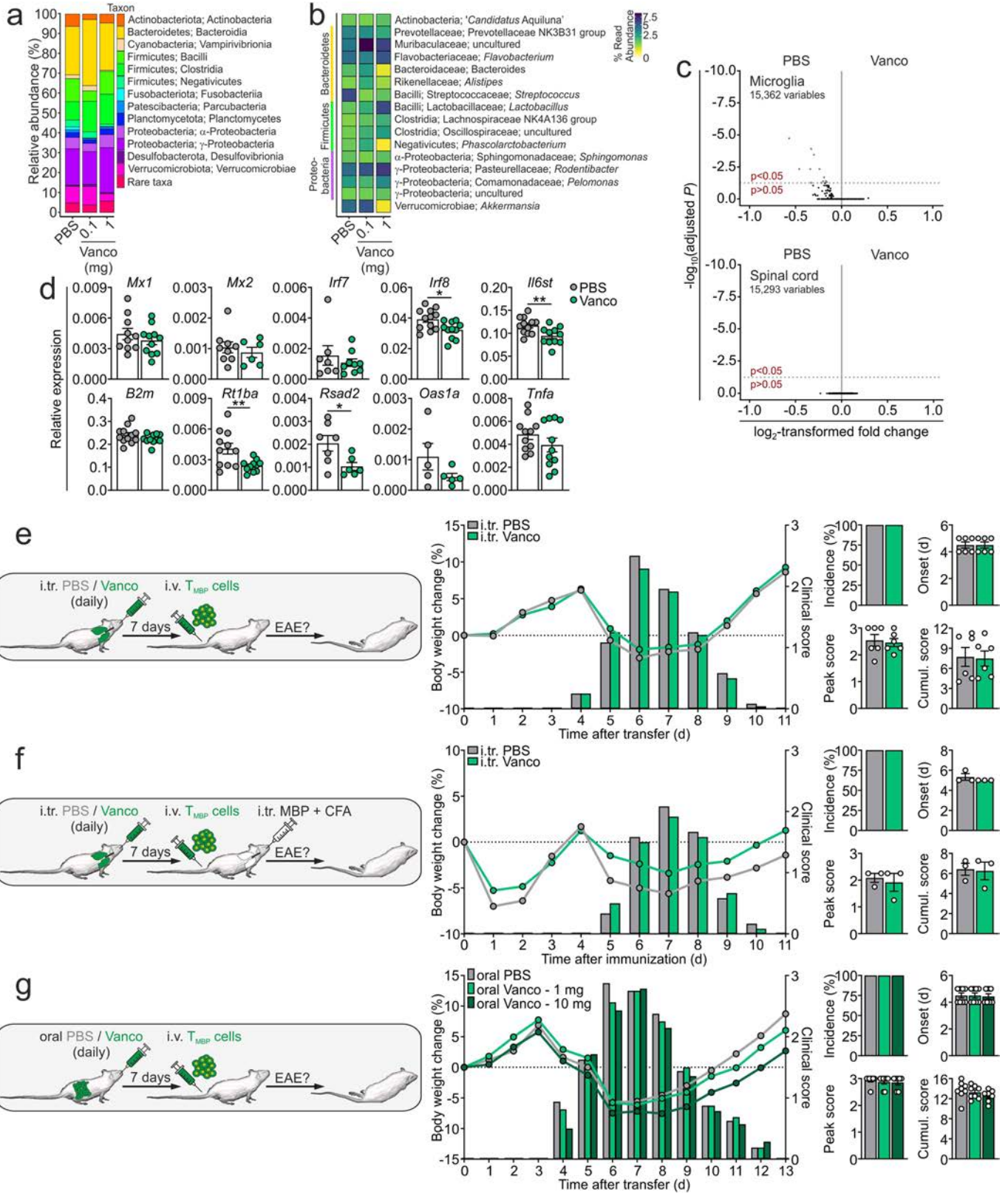
Extended Data Fig. 7 | Lung dysbiosis induces changes in microglial morphology and expression profile. **a**, I.tr. neomycin treatment dampens microglial response in EAE. EAE was induced in rats pre-treated i.tr. with neomycin or PBS by transfer of T_{MBP} cells. Confocal images acquired in spinal cord white matter and grey matter depicting the morphology of Iba1⁺ microglia (red) at the peak of EAE. **b, c**, PLX3397 ameliorates EAE but does not add to the disease-ameliorating effects of i.tr. neomycin treatment. **b**, Quantification of CD45^{low} CD11b⁺ microglia in the brain after 7 days of oral treatment with PLX3397 or vehicle. Flow cytometry. Mean \pm s.e.m. Cumulative data of 3 independent experiments. $n = 9$ (both groups). **c**, Rats were treated orally with PLX3397 or vehicle and i.tr. with neomycin or PBS. After 7 days EAE was induced by transfer of T_{MBP} cells. The treatments were continued throughout the entire disease course. Clinical parameters. Mean \pm s.e.m. Cumulative data of 2 independent experiments. $n = 10$ (vehicle and PBS, vehicle and Neo); $n = 9$ (PLX and PBS); $n = 11$ (PLX and Neo). **d**, I.tr. neomycin treatment does not induce quantitative microglia changes. Rats were treated i.tr. with PBS or neomycin for 7 days. Histological quantification of Iba1⁺ microglia in the grey matter of the spinal cord ($n = 5$ (PBS); $n = 6$ (Neo)), and cytofluorometric quantification of CD45^{low} CD11b⁺ microglia in the spinal cord ($n = 10$ (PBS); $n = 9$ (Neo)). Mean \pm s.e.m. **e, f**, I.tr. neomycin treatment changes microglia morphology in spinal cord and brain cortex without EAE induction. Rats were treated i.tr. with PBS or neomycin for 7 days. **e**, Quantification of the indicated morphological parameters extracted from confocal images of microglia in the spinal cord of PBS- or neomycin-pre-treated rats. Mean \pm s.e.m. 16 cells from 3 different rats per group were analysed. **f**, Iba1⁺ microglia in cortical grey matter after

7 days of i.tr. treatment with PBS or neomycin. Representative confocal 3D-reconstructions and corresponding morphological parameters derived from 13 cells from 3 different rats per group. Mean \pm s.e.m. **g**, I.tr. neomycin treatment induces a type IIFN signature in spinal cord microglia. Significantly enriched ($P < 0.05$) GO terms belonging to biological processes (BP) in genes upregulated in microglia of rats treated with neomycin compared to PBS. **h**, I.tr. neomycin treatment induces type IIFN-stimulated gene expression in brain-derived microglia. Differential expression of the indicated genes in microglial cells sorted from the brain of rats pre-treated with PBS or neomycin. Representative data of 2 independent experiments. Quantitative PCR. Housekeeping gene: β -actin. Mean \pm s.e.m. $n = 5$ (both groups). **i**, I.tr. neomycin treatment induces upregulation of type IIFN-stimulated genes in the total spinal cord. Comparison of differential gene expression between neomycin- and PBS-treated rats. Light red dots, genes significantly upregulated ($P < 0.05$) but below the 0.5-fold change cut-off. Type IIFN-regulated genes are indicated. Bold, genes upregulated in both spinal cord and sorted microglia (Fig. 4b). **j**, Lung dysbiosis does not induce a shift to a type IIFN profile in astrocytes. Expression of type IIFN-regulated genes, β 2MG (*B2m*), MHC-II (*Rt1ba*), and TNF. Note that no signal was detectable in most of the samples. Cumulative data of 2 independent experiments. $n = 6$ (PBS); $n = 7$ (Neo) per condition. **b, d, e, h, j**, Statistical significance determined by unpaired two-tailed *t*-test (Gaussian distribution) and Mann-Whitney test (non-Gaussian distribution). **c**, Statistical significance determined by one-way ANOVA with Tukey's multiple comparisons test. * $P < 0.05$, ** $P < 0.01$, *** $P < 0.001$; ND, not detected.



Extended Data Fig. 8 | Effects of lung dysbiosis on microglia and the lung milieu. **a**, I. tr. neomycin treatment reduces microglial reactivity towards inflammatory cytokines in the CNS. Rats were i. tr. treated daily with neomycin or PBS. After 7 days, PBS or TNF & IFN γ were administered intrathecally (i. th.). Percentage of MHC-II⁺ CD45^{low} CD11b⁺ microglia and number of CD45^{high} CD11b⁺ M Φ in spinal cord and brain 4 h and 18 h after i. th. injection. Flow cytometry. Mean \pm s. e. m. Representative data from 3 independent experiments. For each CNS compartment, $n = 4$ (PBS and PBS); $n = 5$ (PBS and TNF & IFN γ); $n = 3$ (Neo and PBS); $n = 5$ (Neo and TNF & IFN γ). **b**, Lung dysbiosis impairs the capacity of microglia to respond to proinflammatory stimuli in vitro. Microglial cells, isolated from rats treated for 7 days with PBS or neomycin, were stimulated in vitro with increasing doses of IFN γ . Expression of chemokines, cytokines β 2MG (*B2m*), MHC-II (*Rt1ba*) and iNOS (*Nos2*) 4h after stimulation. Quantitative PCR. Representative data of 2 independent experiments. Each value represents the pooled microglia of at least 6 rats per group. **c**, Oral administration of inactivated *P. melaninogenica* does not affect EAE. EAE was induced by transfer of T_{MBP} cells. Clinical parameters after daily

oral treatment started 7 days before T_{MBP} cell transfer and continued throughout the entire disease course. Mean \pm s. e. m. Cumulative data of 2 independent experiments. $n = 5$ (PBS); $n = 4$ (*P. melaninogenica*). **d**, Neomycin treatment increases pulmonary LPS. Concentration of LPS in BALF of rats treated for 7 days with PBS, neomycin or vancomycin (Vanco). ELISA. Mean \pm s. e. m. Cumulative data of 2 independent experiments. $n = 9$ (PBS); $n = 6$ (Vanco); $n = 8$ (Neo). **e**, Neomycin treatment induces a shift to a type I IFN phenotype in pulmonary immune cells. Expression of type I IFN-stimulated genes in pulmonary stromal cells (CD45⁺) and immune cell subsets in PBS- or neomycin-pre-treated rats. Quantitative PCR. Housekeeping gene: β -actin. Mean \pm s. e. m. Cumulative data of 3 independent experiments. $n = 4-13$ (PBS); $n = 4-11$ (Neo) per condition. **a**, **c**, **e**, Statistical significance determined by unpaired two-tailed *t*-test (Gaussian distribution) and Mann-Whitney test (non-Gaussian distribution). **d**, Statistical significance determined by one-way ANOVA with Tukey's multiple comparisons test. * $P < 0.05$, ** $P < 0.01$, *** $P < 0.001$.

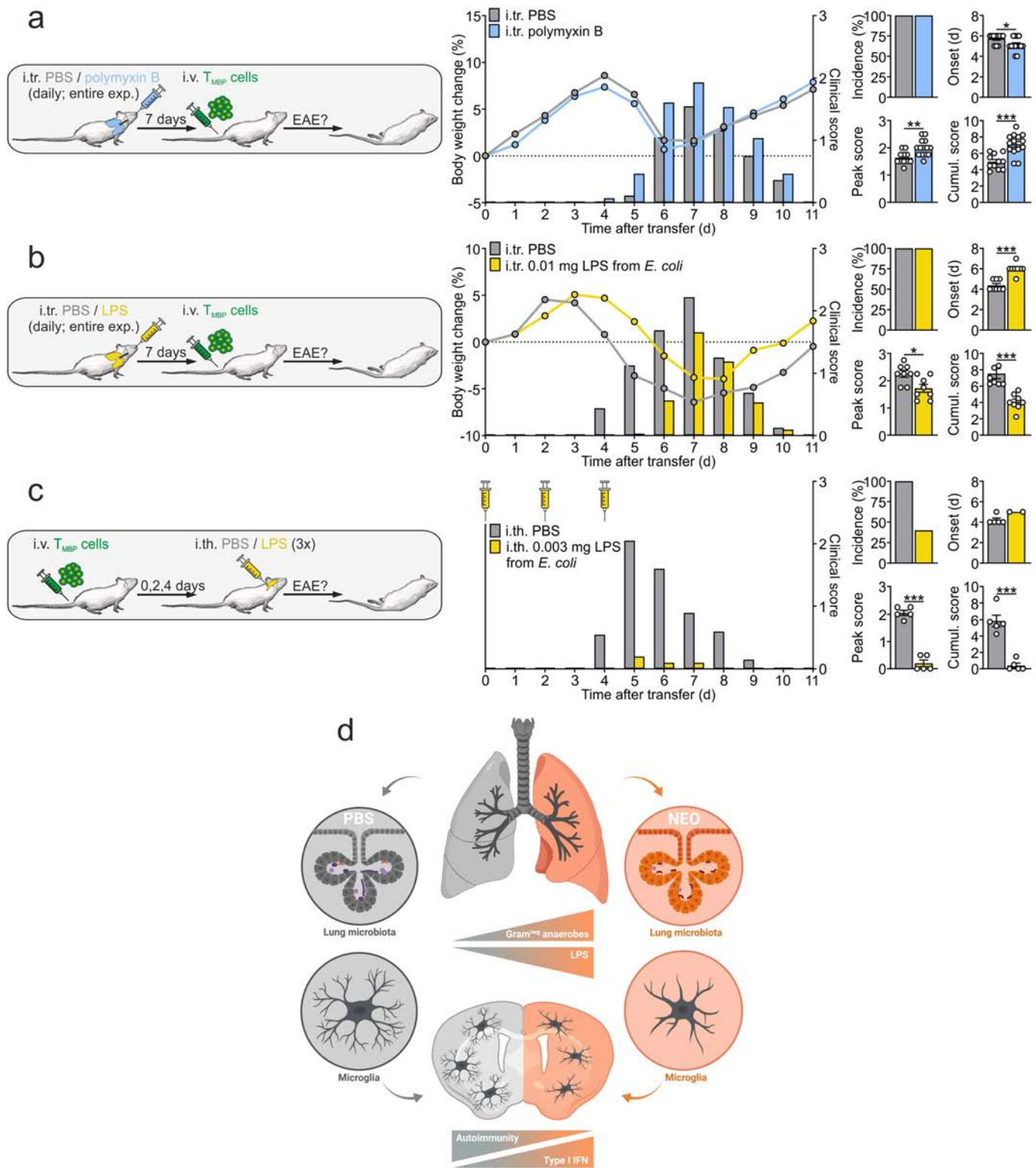


Extended Data Fig. 9 | See next page for caption.

Article

Extended Data Fig. 9 | Vancomycin does not induce a shift towards LPS and does not affect CNS autoimmunity. a, b, Vancomycin does not increase LPS producing phyla in the lung microbiota. **a,** Average relative abundance of bacterial phyla of lung microbiota in rats treated with PBS or vancomycin for 7 days. **b,** Corresponding heat map depicting the most regulated inhabitants of lung microbiota at family level. **c, d,** I.tr. vancomycin treatment does not affect the microglial gene expression profile. **c,** Volcano plots depicting the differential expression profile between vancomycin- and PBS- pre-treated rats in spinal cord derived CD45^{low} CD11b⁺ microglia or in total spinal cord. **d,** Expression of type I IFN-regulated genes in CD45^{low} CD11b⁺ microglial cells isolated from the spinal cord of rats pre-treated i.tr. for 7 days with PBS or vancomycin. Quantitative PCR. Please note that the experiment was performed in parallel with the one depicted in Fig. 4c and therefore the values in the PBS group are the same. Housekeeping gene: β -actin. Mean \pm s.e.m. Cumulative data of 3 independent experiments. $n = 5-12$ (PBS); $n = 5-11$ (Vanco) per

condition. **e, f,** I.tr. vancomycin treatment does not affect transfer EAE or EAE induced via the lung. **e,** Transfer EAE was induced in rats pre-treated i.tr. with PBS or vancomycin for 7 days. Clinical parameters. Mean \pm s.e.m. Representative data of 3 independent experiments. $n = 6$ (both groups). **f,** Lung EAE was induced in rats pre-treated i.tr. with PBS or vancomycin for 7 days. Clinical parameters. Mean \pm s.e.m. Representative data of 3 independent experiments. $n = 3$ (both groups). **g,** Oral treatment with vancomycin does not affect EAE. Transfer EAE was induced in rats pre-treated orally with PBS or vancomycin for 7 days. Clinical parameters. Mean \pm s.e.m. Cumulative data of 2 independent experiments. $n = 8$ (PBS); $n = 8$ (1 mg Vanco); $n = 7$ (10 mg Vanco). **d-f,** Statistical significance determined by unpaired two-tailed t -test (Gaussian distribution) and Mann-Whitney test (non-Gaussian distribution). **g,** Statistical significance determined by one-way ANOVA with Tukey's multiple comparisons test. * $P < 0.05$, ** $P < 0.01$, *** $P < 0.001$.



Extended Data Fig. 10 | LPS regulates EAE severity. **a**, I.tr. treatment with polymyxin B aggravates EAE. Transfer EAE was induced in rats pre-treated i.tr. for 7 days with polymyxin B or PBS. Clinical parameters. Mean \pm s.e.m. Cumulative data of 3 independent experiments. $n = 11$ (PBS); $n = 14$ (polymyxin B). **b**, I.tr. treatment with *E. coli* LPS ameliorates EAE. Transfer EAE was induced in rats pre-treated daily i.tr. for 7 days with LPS or PBS. The treatment was continued throughout the entire disease course. Clinical parameters. Mean \pm s.e.m. Cumulative data of 2 independent experiments. $n = 8$ (both groups).

c, I.th. *E. coli* LPS administration ameliorates EAE. EAE was induced by transfer of T_{MBP} cells. LPS was administered on D0, D2 and D4 after transfer. Clinical parameters. Mean \pm s.e.m. Representative data of 2 independent experiments. $n = 5$ (both groups). **d**, Graphical abstract: Lung microbiota controls the immune reactivity of the CNS in steady state condition and in the case of autoimmunity. Created with BioRender.com. **a-c**, Statistical significance determined by unpaired two-tailed *t*-test (Gaussian distribution) and Mann-Whitney test (non-Gaussian distribution). * $P < 0.05$, ** $P < 0.01$, *** $P < 0.001$.

Reporting Summary

Nature Portfolio wishes to improve the reproducibility of the work that we publish. This form provides structure for consistency and transparency in reporting. For further information on Nature Portfolio policies, see our [Editorial Policies](#) and the [Editorial Policy Checklist](#).

Statistics

For all statistical analyses, confirm that the following items are present in the figure legend, table legend, main text, or Methods section.

n/a Confirmed

- The exact sample size (n) for each experimental group/condition, given as a discrete number and unit of measurement
- A statement on whether measurements were taken from distinct samples or whether the same sample was measured repeatedly
- The statistical test(s) used AND whether they are one- or two-sided
Only common tests should be described solely by name; describe more complex techniques in the Methods section.
- A description of all covariates tested
- A description of any assumptions or corrections, such as tests of normality and adjustment for multiple comparisons
- A full description of the statistical parameters including central tendency (e.g. means) or other basic estimates (e.g. regression coefficient) AND variation (e.g. standard deviation) or associated estimates of uncertainty (e.g. confidence intervals)
- For null hypothesis testing, the test statistic (e.g. F , t , r) with confidence intervals, effect sizes, degrees of freedom and P value noted
Give P values as exact values whenever suitable.
- For Bayesian analysis, information on the choice of priors and Markov chain Monte Carlo settings
- For hierarchical and complex designs, identification of the appropriate level for tests and full reporting of outcomes
- Estimates of effect sizes (e.g. Cohen's d , Pearson's r), indicating how they were calculated

Our web collection on [statistics for biologists](#) contains articles on many of the points above.

Software and code

Policy information about [availability of computer code](#)

Data collection

Cell Quest Pro5.2 (BD)
CytExpert 2.3(Beckman Coulter)
FACS Diva (BD)
VS-ASW (Olympus Corp)
Zen 2012 SP2 (Carl Zeiss) v2.1
OneStep real-time PCR (Applied Biosystems) - v2.3
Magellan (Tecan) - v6.6
MicroBeta TriLux (PerkinElmer Life Sciences)
BZ-II Analyzer Software (Keyence)
Qubit fluorometer (Invitrogen)
iQ™5 Multicolor Real-Time PCR Detection System (BioRad)

Data analysis

CytExpert5.2 (Beckman Coulter)
FIJI image processing software (NIH) - v2.0.0-rc-59/1.51n
Imaris (Bitplane) - v8.0.1
FlowJo (FlowJo LLC) - v.10
Prism (GraphPad Software, Inc) - v6-8
Excel (MicrosoftOffice 2010, v14.0.7208.5000)
Miseq marker gene pipeline v1.8
VSEARCH v2.12.06 a
UNOISE3 algorithm
BLASTn 2.7.1
Rstudio version 1.3.1056 and R 4.0
GMRP v0.1.3

ampvis2 (version 2.6.4)
ggplot2 (v3.3.2)

For manuscripts utilizing custom algorithms or software that are central to the research but not yet described in published literature, software must be made available to editors and reviewers. We strongly encourage code deposition in a community repository (e.g. GitHub). See the Nature Portfolio [guidelines for submitting code & software](#) for further information.

Data

Policy information about [availability of data](#)

All manuscripts must include a [data availability statement](#). This statement should provide the following information, where applicable:

- Accession codes, unique identifiers, or web links for publicly available datasets
- A description of any restrictions on data availability
- For clinical datasets or third party data, please ensure that the statement adheres to our [policy](#)

The datasets generated during and/or analysed during the current study are available in the SRA and the GEO database repository, <https://www.ncbi.nlm.nih.gov/sra/PRJNA789820> and <https://www.ncbi.nlm.nih.gov/geo/query/acc.cgi?acc=GSE192415>. Source data are provided with this paper.

Field-specific reporting

Please select the one below that is the best fit for your research. If you are not sure, read the appropriate sections before making your selection.

Life sciences Behavioural & social sciences Ecological, evolutionary & environmental sciences

For a reference copy of the document with all sections, see [nature.com/documents/nr-reporting-summary-flat.pdf](https://www.nature.com/documents/nr-reporting-summary-flat.pdf)

Life sciences study design

All studies must disclose on these points even when the disclosure is negative.

Sample size	Sample sizes were chosen on the basis of standard power calculations (with $\alpha = 0.05$ and power of 0.8) performed for similar experiments that were previously published. In general, statistical methods were not used to re-calculate or predetermine sample sizes.
Data exclusions	In the microbiota analysis unknown taxa were excluded from the analysis. No other samples were excluded.
Replication	Number of reliable reproductions of each experimental finding is stated in each figure legend.
Randomization	Age and sex matched mice were randomly allocated into experimental groups.
Blinding	Blinding was performed in the assessment of the clinical score. Otherwise blinding was not used since the data collection and the analysis were performed with quantitative instruments to maintaining objectivity.

Behavioural & social sciences study design

All studies must disclose on these points even when the disclosure is negative.

Study description	Briefly describe the study type including whether data are quantitative, qualitative, or mixed-methods (e.g. qualitative cross-sectional, quantitative experimental, mixed-methods case study).
Research sample	State the research sample (e.g. Harvard university undergraduates, villagers in rural India) and provide relevant demographic information (e.g. age, sex) and indicate whether the sample is representative. Provide a rationale for the study sample chosen. For studies involving existing datasets, please describe the dataset and source.
Sampling strategy	Describe the sampling procedure (e.g. random, snowball, stratified, convenience). Describe the statistical methods that were used to predetermine sample size OR if no sample-size calculation was performed, describe how sample sizes were chosen and provide a rationale for why these sample sizes are sufficient. For qualitative data, please indicate whether data saturation was considered, and what criteria were used to decide that no further sampling was needed.
Data collection	Provide details about the data collection procedure, including the instruments or devices used to record the data (e.g. pen and paper, computer, eye tracker, video or audio equipment) whether anyone was present besides the participant(s) and the researcher, and whether the researcher was blind to experimental condition and/or the study hypothesis during data collection.
Timing	Indicate the start and stop dates of data collection. If there is a gap between collection periods, state the dates for each sample cohort.
Data exclusions	If no data were excluded from the analyses, state so OR if data were excluded, provide the exact number of exclusions and the rationale behind them, indicating whether exclusion criteria were pre-established.

Non-participation

State how many participants dropped out/declined participation and the reason(s) given OR provide response rate OR state that no participants dropped out/declined participation.

Randomization

If participants were not allocated into experimental groups, state so OR describe how participants were allocated to groups, and if allocation was not random, describe how covariates were controlled.

Ecological, evolutionary & environmental sciences study design

All studies must disclose on these points even when the disclosure is negative.

Study description

Briefly describe the study. For quantitative data include treatment factors and interactions, design structure (e.g. factorial, nested, hierarchical), nature and number of experimental units and replicates.

Research sample

Describe the research sample (e.g. a group of tagged *Passer domesticus*, all *Stenocereus thurberi* within Organ Pipe Cactus National Monument), and provide a rationale for the sample choice. When relevant, describe the organism taxa, source, sex, age range and any manipulations. State what population the sample is meant to represent when applicable. For studies involving existing datasets, describe the data and its source.

Sampling strategy

Note the sampling procedure. Describe the statistical methods that were used to predetermine sample size OR if no sample-size calculation was performed, describe how sample sizes were chosen and provide a rationale for why these sample sizes are sufficient.

Data collection

Describe the data collection procedure, including who recorded the data and how.

Timing and spatial scale

Indicate the start and stop dates of data collection, noting the frequency and periodicity of sampling and providing a rationale for these choices. If there is a gap between collection periods, state the dates for each sample cohort. Specify the spatial scale from which the data are taken

Data exclusions

If no data were excluded from the analyses, state so OR if data were excluded, describe the exclusions and the rationale behind them, indicating whether exclusion criteria were pre-established.

Reproducibility

Describe the measures taken to verify the reproducibility of experimental findings. For each experiment, note whether any attempts to repeat the experiment failed OR state that all attempts to repeat the experiment were successful.

Randomization

Describe how samples/organisms/participants were allocated into groups. If allocation was not random, describe how covariates were controlled. If this is not relevant to your study, explain why.

Blinding

Describe the extent of blinding used during data acquisition and analysis. If blinding was not possible, describe why OR explain why blinding was not relevant to your study.

Did the study involve field work? Yes No

Field work, collection and transport

Field conditions

Describe the study conditions for field work, providing relevant parameters (e.g. temperature, rainfall).

Location

State the location of the sampling or experiment, providing relevant parameters (e.g. latitude and longitude, elevation, water depth).

Access & import/export

Describe the efforts you have made to access habitats and to collect and import/export your samples in a responsible manner and in compliance with local, national and international laws, noting any permits that were obtained (give the name of the issuing authority, the date of issue, and any identifying information).

Disturbance

Describe any disturbance caused by the study and how it was minimized.

Reporting for specific materials, systems and methods

We require information from authors about some types of materials, experimental systems and methods used in many studies. Here, indicate whether each material, system or method listed is relevant to your study. If you are not sure if a list item applies to your research, read the appropriate section before selecting a response.

Materials & experimental systems

Methods

n/a	Involved in the study
<input type="checkbox"/>	<input checked="" type="checkbox"/> Antibodies
<input type="checkbox"/>	<input checked="" type="checkbox"/> Eukaryotic cell lines
<input checked="" type="checkbox"/>	<input type="checkbox"/> Palaeontology and archaeology
<input type="checkbox"/>	<input checked="" type="checkbox"/> Animals and other organisms
<input checked="" type="checkbox"/>	<input type="checkbox"/> Human research participants
<input checked="" type="checkbox"/>	<input type="checkbox"/> Clinical data
<input checked="" type="checkbox"/>	<input type="checkbox"/> Dual use research of concern

n/a	Involved in the study
<input checked="" type="checkbox"/>	<input type="checkbox"/> ChIP-seq
<input type="checkbox"/>	<input checked="" type="checkbox"/> Flow cytometry
<input checked="" type="checkbox"/>	<input type="checkbox"/> MRI-based neuroimaging

Antibodies

Antibodies used

The following anti-rat mAbs were used for surface staining: abTCR-AF647 (clone R73, Biolegend), CD45RA-PE (clone OX-33; Biolegend), CD8 α -FITC (OX-8; Biolegend) and CD8 α -PerCP (BD Biosciences), CD4-PE/Cy7 and CD4-PE/Cy5 (Clone W3/25; both BD Biosciences), CD134-BV421 (Clone OX40, BD Biosciences), CD25-PE (Clone OX39 Biolegend), CD62L-PE (clone OX85, Biolegend), LFA-1-APC (integrin α L, clone WT.1, Serotec), VLA-4-APC (anti-CD49d, clone TA-2, Sigma-Aldrich), CD31-PE (clone TLD-3A12, BD Biosciences), CD11b/c-PE and CD11b/c APC (clone OX-42, Biolegend), CD45-PE, CD45-AF647 and CD45-PerCP (clone OX-1; all Biolegend), GLAST-APC (ACSA1, Miltenyi), RT1B-FITC (clone OX-6, BD Biosciences), RP3-BV421 (BD Biosciences), CD172a-FITC (Clone ED9, Bio-Rad). Matching directly labelled mouse IgM (clone R6-60.2, BD Biosciences), mouse IgG-APC (Jackson) and Mouse IgG1k (MOPC 31C, Sigma-Aldrich) were used as isotype controls.

For intracellular staining the following antibodies were used: rat anti-mouse anti-IL17-BV42 (clone TC11-8H4, Biolegend), mouse anti-rat IFN γ -PE (Clone DB1, Biolegend) and anti-mouse/rat/human FoxP3-PE (Biolegend).

For histological analysis anti-Iba-1 (Rabbit; polyclonal; Wako 019-19741) and Rhodamine RedTM-X (RRX) anti-rabbit (Donkey; polyclonal; Jackson 711-295-152) were used as first and secondary antibody, respectively.

Validation

All antibodies used in this study were from commercial vendors and were validated for the specific application (immunohistochemistry, flow cytometry/cell sorting) by the manufacturers. The validation is reported on their websites.

Eukaryotic cell lines

Policy information about [cell lines](#)

Cell line source(s)

GP+E86 ecotropic retroviral packaging cell line (ATCC).
 Primary Lewis rat CD4 effector T cells specific for myelin basic protein (Establishment protocol reported in METHODS).
 Primary Lewis rat CD4 effector T cells specific for beta-synuclein (Establishment protocol reported in METHODS).
 Primary Lewis rat CD4 effector T cells specific for ovalbumin (Establishment protocol reported in METHODS).
 Primary microglial cells (Establishment protocol reported in METHODS).

Authentication

No authentication was performed for GP+E86 and derivative cell lines.
 For T cell lines, authentication reported in METHODS.

Mycoplasma contamination

All used cell lines were tested negative for mycoplasma contamination.

Commonly misidentified lines
(See [ICLAC](#) register)

No commonly misidentified cell lines were used in the study

Animals and other organisms

Policy information about [studies involving animals](#); [ARRIVE guidelines](#) recommended for reporting animal research

Laboratory animals

Lewis rats on a LEW/CrI background were bred at the animal facility of the University Medical Centre Göttingen (Germany) or obtained from Charles River (Germany). T cell receptor transgenic Lewis rat strain (ubiquitous expression of GFP-TCRa-TCRb transgene; unknown integration site) specific for beta-synuclein antigen were previously generated in our lab (Lodygin et al., Nature 2019) and maintained at the animal facility of University Medical Center Göttingen. Male and female 6 – 10 weeks old animals were used for all experiments. No differences between the sexes were observed.

Wild animals

The study did not involve wild animals

Field-collected samples

The study did not involve samples collected from the field

Ethics oversight

All animal experiments were approved by the animal welfare of Lower Saxony, Germany.

Note that full information on the approval of the study protocol must also be provided in the manuscript.

Plots

Confirm that:

- The axis labels state the marker and fluorochrome used (e.g. CD4-FITC).
- The axis scales are clearly visible. Include numbers along axes only for bottom left plot of group (a 'group' is an analysis of identical markers).
- All plots are contour plots with outliers or pseudocolor plots.
- A numerical value for number of cells or percentage (with statistics) is provided.

Methodology

Sample preparation

EDTA-treated blood was retrieved from the heart by cardiac puncture. Mononuclear cells were isolated by density gradient using Lymphocyte Separation Medium (PromoCell; centrifugation settings: 30 min at 840xg and 20°). Lungs were thoroughly and repeatedly sectioned using a tissue chopper (Mcllwain). The homogenized tissue was washed with EH. Pellets were re-suspended and incubated with 2 mL of 0.3 % collagenase in PBS for 30 min at 37 °C under constant shaking. Subsequently, the tissue was homogenized using a gentleMACS Dissociator (Miltenyi Biotec), forced through a cell strainer (40 µm) and washed with EH. The pellet was re-suspended in 5 mL 40 % isotonic percoll and underlayered with 5 mL 70 % percoll (centrifugation settings: 30 min at 2000 rpm and 4°). The leukocyte-enriched interphase was then collected, washed and re-suspended in EH medium. Spleens and lymph nodes were passed through a cell strainer (40 µm), washed once with PBS and treated with ACK-buffer for erythrocyte lysis. Parenchyma and leptomeninges of brain and spinal cord were passed through a cell strainer (40 µm) and washed once with PBS. Myelin debris was eliminated by Percoll-density gradient (centrifugation settings: 30 min at 700xg and 4 °C). For endothelial cell isolation, spinal cords were dissected, and the meninges were removed from the parenchyma. Spinal cord parenchyma were brought to single cell suspension using a Dounce homogenizer. The meninges were chopped up using a razor blade. The CNS tissues were then digested with liberase (0.4 U/ mL; Roche) and DNase I (120 U/mL; Roche) at 37 °C for 1 h with gentle pipetting of the solution every 10 min. Subsequently, the cell suspension was passed through a 40 µm cell strainer. Myelin debris was removed using a Percoll-density gradient as described above. Single cell population were used for surface and intracellular staining.

For surface staining the cell were antibody labeled with a mix of primary antibodies described in the list above for 30 minutes at 4°, washed by PBS and FACS-analyzed.

For intracellular detection of IFN-gamma and IL17, ex vivo isolated cells were left unstimulated or stimulated in vitro with 1 µg/mL PMA (Phorbol 12-myristate 13-acetate, Sigma-Aldrich) and 5 µM Ionomycin calcium salt (Sigma-Aldrich) for 30 minutes. Brefeldin A (5 µg/mL) was added to block cytokine secretion. Cell were cultured for further 2 h and surface stained with anti-rat αβTCR-AlexaFluor647 (Clone R73, Biolegend), anti-rat CD4-PE/Cy7 (Clone W3/25, Biolegend) and anti-CD8α-PerCP (Clone OX-8, Biolegend) for 30 minutes at 4°C. The cells were fixed with 2 % PFA, permeabilized with BD Perm/Wash buffer (BD Biosciences) and stained with rat anti-mouse anti-IL17-BV42 (clone TC11-8H4, Biolegend) and mouse anti-rat IFNγ-PE (Clone DB1, Biolegend) for 45 minutes at 4°C. For intracellular staining for FoxP3 detection, ex vivo isolated cells were surface-stained as described above, fixed and permeabilized using FoxP3/transcription factors staining buffer set (eBioscience) following the manufacturer's instructions and stained with anti-mouse/rat/human FoxP3-PE (Biolegend).

Instrument

BD FACSCalibur, BD FACS Aria II, Beckman Coulter CytoFLEX S

Software

BD CellQuest Pro5.2, BD FACS Diva software or Beckman Coulter CytExpert2.3 were used for acquisition of flow cytometry data, Flowjo-V10 and Beckman Coulter CytExpert2.3 for data analysis.

Cell population abundance

For sequencing analysis of myelin-reactive T cells retrieved from the lungs of NEO- or PBS-treated animals on D0 and D1 post i.tr. immunization 20000 cells were sorted for each replicate. Each sample was re-analysed after sorting for assessing cell population abundance and purity. Just samples with a purity > 98% were further processed.

For sequencing analysis of total spinal cord tissue or from spinal cord derived CD45low CD11b+ microglial cells isolated from animals treated with PBS, Vancomycin or Neomycin between 20,000 and 40,000 cells were sorted for each replicate. Just samples with a purity > 98% were further processed.

Each sample was re-analysed after sorting for assessing cell population abundance and purity.

Gating strategy

Gating strategy, with representative gating, is reported in Supplementary Fig. 1.

Briefly, singlets were gated using the height, area and the pulse width of the forward and side scatter. The boundaries between "positive" and "negative" were determined by the clear cell subpopulations and unstained negative controls.

- Tick this box to confirm that a figure exemplifying the gating strategy is provided in the Supplementary Information.